Int. J. Solids Structures Vol. 30, No. 5, pp. 695–723, 1993
Printed in Great Britain

0020–7683/93 $6.00+.00

ON THE DEVELOPMENT OF VARIABLE-SEPARABLE ASYMPTOTIC ELASTOPLASTIC SOLUTIONS FOR INTERFACIAL CRACKS

S. M. SHARMA and N. ARAVAS
Department of Mechanical Engineering and Applied Mechanics,
University of Pennsylvania, Philadelphia, PA 19104, U.S.A.

(*Received* 10 *June* 1991; *in revised form* 14 *August* 1992)

Abstract—The problem of a plane strain crack lying along the interface between an elastic–plastic power-law hardening material and a rigid substrate is analysed in detail. The possibility of elastoplastic asymptotic crack tip solutions that are separable in r and θ is explored, where (r, θ) are polar coordinates at the crack tip. It is found that such variable-separable solutions do exist, and the first two terms in the asymptotic expansion of the stress and displacement fields in the near-tip region are obtained. It is shown that both the first and the second terms in the stress expansion are singular in r as $r \to 0$. The asymptotic solution is studied in detail for values of the hardening exponent n near $n = 1$ via a small perturbation of the governing equations about the linear problem; it is shown that the leading and second order singular terms in the stress expansion branch from the mode-I and mode-II linear elastic solutions respectively. The predictions of the asymptotic solution are compared with the results of detailed finite element calculations. The region of dominance of the asymptotic solution is found to depend strongly on the geometry of the structure considered and the type of the applied loading.

1. INTRODUCTION

The problem of interfacial fracture has received a lot of attention recently and numerous publications addressing the mechanics of it have appeared in the literature. The *elastic* interface crack problem is now well understood and a complete bibliography on the subject can be found in the review articles by Rice (1988), Comninou (1990), Hutchinson (1990), Shih (1991) and Hutchinson and Suo (1992). However, several aspects of the *elastic–plastic* problem are not as clear yet and a few conflicting solutions have been published. Yuli Gao and Zhiwen Lou (1990) considered the problem of a plane strain crack lying along the interface of two elastic–plastic power-law hardening materials and presented asymptotic solutions in which the near tip stress and deformation fields are separable functions in r and θ, (r, θ) being polar coordinates at the crack tip; their asymptotic solutions involve two arbitrary constants, so that the near tip mode-mix (ratio of opening to shearing stresses on the interface) can be arbitrary. The same problem was also analysed by Wang (1990) and Champion and Atkinson (1991) who presented asymptotic solutions different from those of Yuli Gao and Zhiwen Lou; these solutions are also variable-separable as $r \to 0$, but involve only one arbitrary multiplicative constant, so that the near tip mode-mix is completely defined by the asymptotic solution in terms of the larger hardening exponent of the two power-law hardening materials. A variable-separable elastoplastic asymptotic solution for the interface crack in anti-plane shear has been developed by Champion and Atkinson (1990). Numerical solutions to the elastoplastic interface crack problem have been presented by Shih and Asaro (1988, 1989, 1991) who carried out detailed finite element calculations for different specimen geometries and loading conditions. The problem of the interface crack along the interface between an elastic-perfectly-plastic material and a rigid substrate has been analysed by Quanxin Guo and Keer (1990) and Zywicz and Parks (1992) who presented several possible slip line fields for the near crack tip region.

The question of near tip material interpenetration and possible contact of the crack faces has been addressed by Zywicz and Parks (1990), who developed a slip line field solution for a perfectly plastic material, and by Aravas and Sharma (1991), who used a power-law hardening material model and obtained asymptotic elastoplastic solutions for the interface crack with contact zones.

A thorough analysis of the plane strain elastoplastic interfacial crack problem is presented herein. The crack lies along the interface between an elastoplastic continuum and a rigid substrate and the crack faces are assumed to be traction free (open crack). J_2-deformation theory with power-law hardening is used to describe the constitutive behavior of the materials involved. We attempt an asymptotic expansion of the stress field $\boldsymbol{\sigma}$ of the form

$$\boldsymbol{\sigma}(r,\theta) = (r/J)^s \boldsymbol{\sigma}^{(0)}(\theta) + Q r^t \boldsymbol{\sigma}^{(1)}(\theta) + \cdots \quad \text{as} \quad r \to 0, \tag{1}$$

where $\boldsymbol{\sigma}^{(0)}$ and $\boldsymbol{\sigma}^{(1)}$ are normalized angular functions, $s < t < \cdots$, J is the J-integral, and Q is a parameter that controls the magnitude of the second term and depends on the type and magnitude of the applied loads as well as on the geometry under consideration. Both the leading and the second order terms in eqn (1) are determined. Our results for the leading term $\boldsymbol{\sigma}^{(0)}$ agree with those of Wang (1990) and Champion and Atkinson (1991); we have been unable, however, to reproduce the solutions of Yuli Gao and Zhiwen Lou (1990). In the above asymptotic expansion of the near tip stresses $s = -1/(n+1)$, and the second exponent t is also *negative*, i.e. $s < t < 0$, for all values of the hardening exponent n.

The leading order solution involves only one multiplicative constant, the J-integral, and the ratio $\sigma^{(0)}_{\theta\theta}/\sigma^{(0)}_{r\theta}$ on the interface is completely defined by the asymptotic solution for a given value of the hardening exponent. It is found that the leading order solution $\boldsymbol{\sigma}^{(0)}$ corresponds to a dominating tensile mode ahead of the crack for all values of the hardening exponent n. This result appears, at first, to be unexpected, since the corresponding asymptotic solution for an incompressible linear elastic material ($n = 1$) contains two arbitrary constants, thus admitting an arbitrary mode-mix. However, Champion and Atkinson (1991), using a small perturbation technique, were able to show analytically that, for values of n slightly larger than 1, the resulting non-linear eigenvalue problem that defines $\boldsymbol{\sigma}^{(0)}$ has only one independent eigensolution, which branches from the mode-I solution as n increases from 1 and uniquely defines the near tip mode-mix in terms of n. The source of the discreteness of the asymptotic mode-mix is discussed thoroughly in a recent article by Bose and Ponte Castañeda (1992), who list several "degenerate" (arbitrary mode-mix) and "non-degenerate" (fixed mode-mix) eigenvalue problems in the mechanics of stationary and propagating cracks. It should also be noted that, even in the context of linear elasticity, it is possible to have asymptotic crack tip solutions in which the mode-mix is completely defined by the asymptotic solution itself; an example of this is presented in Section 2 below.

The second order solution in (1) is singular in r, i.e. $t < 0$, and $\boldsymbol{\sigma}^{(1)}$ has a substantial shearing component ahead of the crack. In Section 4, we study the behavior of the second term in the stress expansion (1) via a small perturbation of n about $n = 1$, and show analytically that $\boldsymbol{\sigma}^{(1)}(\theta)$ branches from the mode-II linear elastic solution. It is also shown that in weakly non-linear materials (say $n = 1+\epsilon$, ϵ = small), the difference between the two stress exponents s and t is of order ϵ^2, i.e. $t = s + O(\epsilon^2)$ near $n = 1$. A practical implication of this is that, for finite (but small) values of r, the second term in the stress expansion becomes important and does affect the near tip mode-mix. Put in other words, the value of the ratio $(\sigma_{\theta\theta}/\sigma_{r\theta})_{\theta=0}$ near the crack tip depends on both J and Q. Therefore, J and Q can be viewed as the non-linear counterparts of the mode-I and mode-II stress intensity factors of the linear elastic solution.

The predictions of the developed elastoplastic asymptotic solutions are compared with the results of detailed finite element calculations under small- as well as large-scale-yielding conditions. The region of dominance of the elastoplastic asymptotic solution is found to depend strongly on the magnitude and type of applied loading as well as on the geometry considered.

2. TWO LINEAR ELASTIC SOLUTIONS

In this section, we demonstrate, by means of two simple problems, that in the context of linear elasticity the near tip mode-mix may or may not be determined by the asymptotic solution alone, depending on the problem under consideration.

We consider two different models for the near tip region of a plane strain interfacial crack along a *rigid substrate*, where perfect bonding is assumed for the attached part of the interface: (i) the traditional open crack tip model as formulated by Williams (1959), and (ii) Comninou's (1977) closed crack-tip model, in which the crack surfaces are assumed to be in frictionless contact near the tip.

The linear elastic solution of the first problem is known to be non-separable in r and θ, unless the material is incompressible. In order to simplify the solution, we assume that Poisson's ratio is indeed equal to 0.5. In such a case, the near tip solution is of the form of eqn (1), where the leading order exponent s and the angular function $\boldsymbol{\sigma}^{(0)}$ are determined from the solution of a linear eigenvalue problem. It can be readily shown that the leading eigenvalue is $s = -1/2$, and that there are *two* linearly independent eigenfunctions corresponding to the mode-I and mode-II solutions respectively. In view of the linearity of the problem, the general leading order solution is found to be (Erdogan, 1963; Salganik, 1963; England, 1965; Rice and Sih, 1965)

$$\sigma_{xx} = \frac{1}{4\sqrt{2\pi r}}\left[K_{\mathrm{I}}\left(3\cos\frac{\theta}{2}+\cos\frac{5\theta}{2}\right)+K_{\mathrm{II}}\left(-7\sin\frac{\theta}{2}-\sin\frac{5\theta}{2}\right)\right], \tag{2}$$

$$\sigma_{yy} = \frac{1}{4\sqrt{2\pi r}}\left[K_{\mathrm{I}}\left(5\cos\frac{\theta}{2}-\cos\frac{5\theta}{2}\right)+K_{\mathrm{II}}\left(-\sin\frac{\theta}{2}+\sin\frac{5\theta}{2}\right)\right], \tag{3}$$

and

$$\sigma_{xy} = \frac{1}{4\sqrt{2\pi r}}\left[K_{\mathrm{I}}\left(-\sin\frac{\theta}{2}+\sin\frac{5\theta}{2}\right)+K_{\mathrm{II}}\left(3\cos\frac{\theta}{2}+\cos\frac{5\theta}{2}\right)\right], \tag{4}$$

where the crack-tip coordinate system shown in Fig. 1 is used. Equations (2)–(4) show that the asymptotic solution involves two arbitrary constants, K_{I} and K_{II}, so that the near tip mode-mix cannot be defined by the asymptotic solution alone.

We turn next to Comninou's model and relax the incompressibility assumption. Again, s and $\boldsymbol{\sigma}^{(0)}$ are determined from the solution of an eigenvalue problem. The leading eigenvalue is $s = -1/2$; in this case, however, there is *only one* independent eigenfunction, and the leading order solution can be written as

$$\sigma_{xx} = -\frac{K_{\mathrm{II}}^{\mathrm{c}}}{\sqrt{2\pi r}}\frac{1}{2(\kappa+1)}\left[(2\kappa+5)\sin\frac{\theta}{2}+\sin\frac{5\theta}{2}\right], \tag{5}$$

$$\sigma_{yy} = \frac{K_{\mathrm{II}}^{\mathrm{c}}}{\sqrt{2\pi r}}\frac{1}{2(\kappa+1)}\left[(2\kappa-3)\sin\frac{\theta}{2}+\sin\frac{5\theta}{2}\right], \tag{6}$$

and

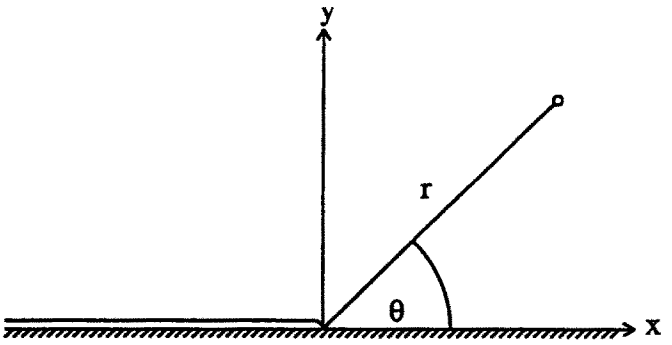

Fig. 1. Schematic representation of the crack-tip region.

$$\sigma_{xy} = \frac{K_{II}^{e}}{\sqrt{2\pi r}} \frac{1}{2(\kappa+1)} \left[(2\kappa+1)\cos\frac{\theta}{2} + \cos\frac{5\theta}{2} \right], \tag{7}$$

where $\kappa = 3-4\nu$ for plane strain. The near tip mode-mix is determined by the asymptotic solution itself; in fact, the asymptotic solution is mode-II-like, in the sense that the shear stress is the only singular stress component along the interface as $r \to 0$.

3. ASYMPTOTIC VARIABLE-SEPARABLE ELASTOPLASTIC SOLUTIONS

We consider the plane strain problem of a crack lying along the interface of a homogeneous medium and a rigid substrate. The crack face is assumed to be traction free. The constitutive behavior of the deformable medium is characterized by the J_2 deformation theory for a Ramberg–Osgood uniaxial stress–strain behavior, namely

$$\epsilon_{ij} = \frac{1+\nu}{E} s_{ij} + \frac{1-2\nu}{3E} \sigma_{kk}\delta_{ij} + \tfrac{3}{2}\alpha\epsilon_0 \left(\frac{\sigma_e}{\sigma_0}\right)^{n-1} \frac{s_{ij}}{\sigma_0}, \tag{8}$$

where ϵ is the infinitesimal strain tensor, $\mathbf{s}$ is the stress deviator, δ_{ij} is the Kronecker delta, E is Young's modulus, ν is Poisson's ratio, α is a material constant, n is the hardening exponent ($1 \leqslant n \leqslant \infty$), σ_0 is the yield stress, $\epsilon_0 = \sigma_0/E$ and σ_e is the von Mises equivalent stress defined as $\sigma_e = (1.5 s_{ij} s_{ij})^{1/2}$.

Under plane strain conditions, the non-zero stress, strain and displacement components are σ_{rr}, $\sigma_{\theta\theta}$, $\sigma_{r\theta}$, σ_{zz}, ϵ_{rr}, $\epsilon_{\theta\theta}$, $\epsilon_{r\theta}$, u_r and u_θ, where r and θ are crack-tip polar coordinates as shown in Fig. 1, and z is the coordinate axis normal to the plane of deformation.

The boundary conditions for the asymptotic problem are (see Fig. 1)

$$u_r(r,0) = 0, \quad u_\theta(r,0) = 0 \quad \text{as} \quad r \to 0, \tag{9}$$

$$\sigma_{\theta\theta}(r,\pi) = 0, \quad \sigma_{r\theta}(r,\pi) = 0 \quad \text{as} \quad r \to 0. \tag{10}$$

The asymptotic solution is obtained using the technique developed recently by Sharma and Aravas (1991a), which is outlined briefly in the following. The problem is formulated in terms of fundamental quantities, namely stresses and displacements, and an asymptotic expansion of the form of eqn (1) is attempted. Using a J-integral argument similar to that used by Hutchinson (1968) and Rice and Rosengren (1968), we conclude that $s = -1/(n+1)$. For the purposes of clarity, the stress expansion is rewritten as

$$\frac{\boldsymbol{\sigma}(r,\theta)}{\sigma_0} = \left(\frac{J}{\alpha\epsilon_0\sigma_0 I_n r}\right)^{1/(n+1)} \tilde{\boldsymbol{\sigma}}^{(0)}(\theta) + Q\left(\frac{r}{J/\sigma_0}\right)^{t} \tilde{\boldsymbol{\sigma}}^{(1)}(\theta) + \cdots, \tag{11}$$

where J is the J-integral, and Q is a dimensionless constant that controls the magnitude of the second stress term. It can be readily shown that the corresponding displacement expansion is of the form (Sharma and Aravas, 1991a)

$$\frac{\mathbf{u}(r,\theta)}{\alpha\epsilon_0} = \left(\frac{J}{\alpha\epsilon_0\sigma_0 I_n}\right)^{n/(n+1)} r^{1/(n+1)} \tilde{\mathbf{u}}^{(0)}(\theta) + \frac{Q}{(J/\sigma_0)^t} \left(\frac{J}{\alpha\epsilon_0\sigma_0 I_n}\right)^{(n-1)/(n+1)} r^{s(n-1)+t+1} \tilde{\mathbf{u}}^{(1)}(\theta) + \cdots, \tag{12}$$

provided that $t < (n-2)/(n+1)$. In the above equations, I_n is defined as

$$I_n = \int_0^{\pi} \left[\frac{n}{n+1} \tilde{\sigma}_e^{(0)^{n+1}} \cos\theta - n_i \tilde{\sigma}_{ij}^{(0)} \left(\frac{1}{n+1} \tilde{u}_j^{(0)} \cos\theta - \frac{\mathrm{d}\tilde{u}_j^{(0)}}{\mathrm{d}\theta} \sin\theta \right) \right] \mathrm{d}\theta, \tag{13}$$

where $n_1 = \cos\theta, n_2 = \sin\theta$ and the components $\tilde{\sigma}_{ij}^{(0)}$ and $\tilde{u}_i^{(0)}$ are understood to be Cartesian (versus polar).

The expansions (11) and (12) are then substituted into the governing equations of equilibrium and the stress–strain relation (8); terms having like powers of r are collected, and a hierarchy of problems is obtained. The leading order problem that defines $\tilde{\boldsymbol{\sigma}}^{(0)}$ and $\tilde{\mathbf{u}}^{(0)}$ consists of a set of five non-linear ordinary differential equations; the next order problem is a linear eigenvalue problem that defines the second stress exponent t and the eigenfunctions $\tilde{\boldsymbol{\sigma}}^{(1)}$ and $\tilde{\mathbf{u}}^{(1)}$. The leading as well as the second order problems are solved numerically for different values of the hardening exponent using a one-dimensional Galerkin-finite-element technique. More details on the formulation and the computations are reported in Sharma and Aravas (1991a) and will not be repeated here.

The angular variations of the leading order in-plane stress and displacement components for $n = 5, 10$ and 50 are shown in Fig. 2. The solutions are normalized so that $(1.5\tilde{s}_{ij}^{(0)}\tilde{s}_{ij}^{(0)})_{\max}^{1/2} = 1$, and $\tilde{u}_\theta^{(0)}(\pi) < 0$ (open crack). The solutions obtained agree well with those reported by Wang (1990) and Champion and Atkinson (1991). The stress distribution for $n = 50$ closely approximates one of the slip line fields developed by Zywicz and Parks (1992) shown in Fig. 3.

The dependence of I_n on the hardening exponent n is shown in Fig. 4.

The solutions shown in Fig. 2 are obtained by solving the leading order system of the homogeneous non-linear differential equations, as described by Sharma and Aravas (1991a), together with the boundary conditions (9) and (10), *without* specifying the mode-mix ahead of the crack. Put in other words, the asymptotic solutions obtained involve *only one* arbitrary constant (the J-integral). This contrasts with the asymptotic elastoplastic crack tip solutions in homogeneous media, where two arbitrary constants are involved, thus admitting an arbitrary mode-mix ahead of the crack (Shih, 1974). It should be noted that we did try to develop solutions with an arbitrary mode-mix for the interface crack problem by assigning arbitrary values to the ratio $\tilde{\sigma}_{\theta\theta}^{(0)}/\tilde{\sigma}_{r\theta}^{(0)}$ on $\theta = 0$, in addition to the boundary conditions (9) and (10); in that case, however, the Newton–Raphson method used for the solution of the discretized form of the leading order system of equations failed to converge and we were unable to obtain any solutions. In this connection, we mention that the two-constant (arbitrary mode-mix) solutions presented by Yuli Gao and Zhiwen Lou (1990) are questionable, since they violate the condition $\tilde{\sigma}_{rr}^{(0)} = \tilde{\sigma}_{\theta\theta}^{(0)}$ on $\theta = 0$, which results from the fact that $\epsilon_{rr} = 0$ along the interface.

The angular variation of the second order stress and displacement components for $n = 5$, 10 and 50 are shown in Fig. 5. The solutions are normalized so that $(1.5\tilde{s}_{ij}^{(1)}\tilde{s}_{ij}^{(1)})_{\max}^{1/2} = 1$, and $\tilde{u}_\theta^{(1)}(\pi) < 0$.

The variation of the two stress components (s, t) with the hardening exponent n is shown in Fig. 6. The values of the second stress exponent t are listed in Table 1 for integer values of the hardening exponent n in the region $2 \leqslant n \leqslant 20$. It should be noted that t is *negative* for all values of n and close to the leading order exponent $s = -1/(n+1)$, i.e. both the first and the second term in the stress expansion (11) are singular as $r \to 0$. This indicates that the contribution of the second term on the right hand side of (11) is important even for small values of r. For the representative values of $n = 3$, 5 and 10 the corresponding exponents are

$$n = 3, \quad s = -0.250, \quad t = -0.212,$$
$$n = 5, \quad s = -0.167, \quad t = -0.113,$$

and

$$n = 10, \quad s = -0.091, \quad t = -0.037.$$

Notice that the first decimal point in s and t is the same for all values of the hardening

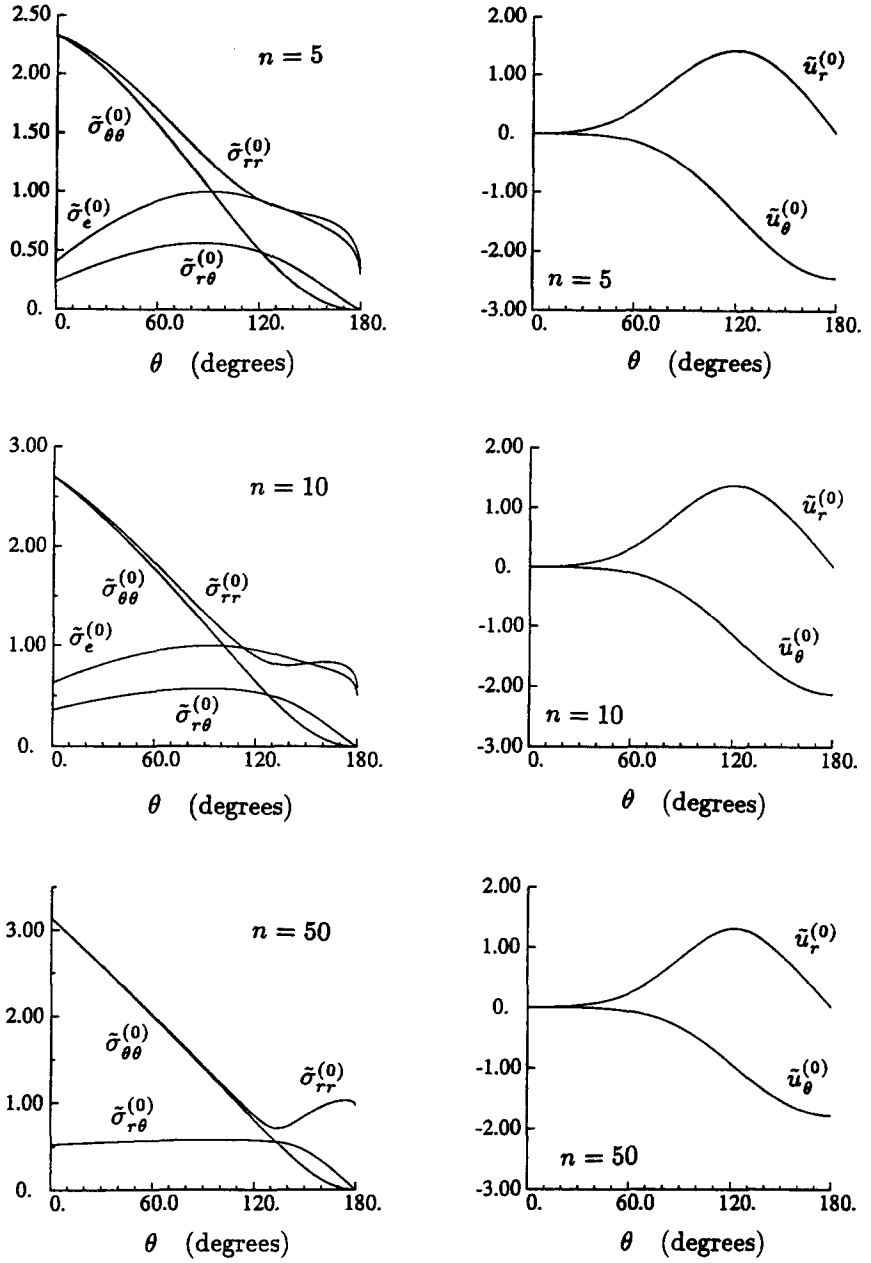

Fig. 2. Angular variation of the leading order in-plane stress and displacement components for $n = 5$, 10 and 50.

exponent n. In the following section, we show that, for a weakly non-linear material (say $n = 1+\epsilon$, ϵ = small), the difference between t and s is of order ϵ^2, i.e. $t = s+O(\epsilon^2)$ near $n = 1$ (see also Fig. 6).

Next, we consider the crack tip "mode-mix parameter" $M_p^{(0)}$, which is defined as (Shih, 1974)

$$M_p^{(0)} = \frac{2}{\pi}\tan^{-1}\left(\lim_{r\to 0}\frac{\sigma_{\theta\theta}}{\sigma_{r\theta}}\right)_{\theta=0} = \frac{2}{\pi}\tan^{-1}\left(\frac{\tilde{\sigma}_{\theta\theta}^{(0)}}{\tilde{\sigma}_{r\theta}^{(0)}}\right)_{\theta=0}. \tag{14}$$

The possible values of $M_p^{(0)}$ range from 0 (mode-II) to ± 1 (mode-I). In order to study the

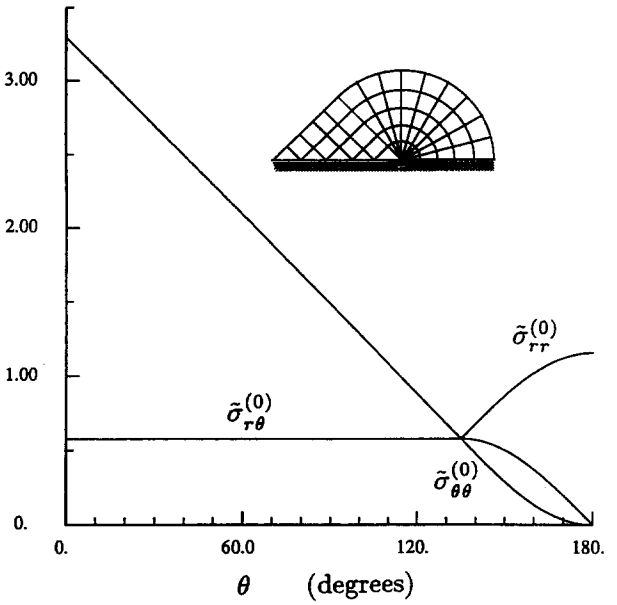

Fig. 3. Slip line solution.

nature of the second term in the stress expansion, we introduce the second-order mode-mix $M_p^{(1)}$ defined as

$$M_p^{(1)} = \frac{2}{\pi} \tan^{-1} \left(\frac{\tilde{\sigma}_{\theta\theta}^{(1)}}{\tilde{\sigma}_{r\theta}^{(1)}} \right)_{\theta=0}. \tag{15}$$

The variation of the determined $M_p^{(0)}$ and $M_p^{(1)}$ with the hardening exponent n is plotted in Fig. 7. We observe that the values of $M_p^{(0)}$ are close to 1, indicating that the crack opening mode is the dominant mode ahead of the crack tip. The second-order mode-mix $M_p^{(1)}$ takes values between 0 and -1, and has a substantial mode-II component, especially for values of n near $n = 1$.

The results shown in Figs 6 and 7 make it clear that the first and second terms in the stress expansion (11) branch from the mode-I and mode-II linear elastic solutions,

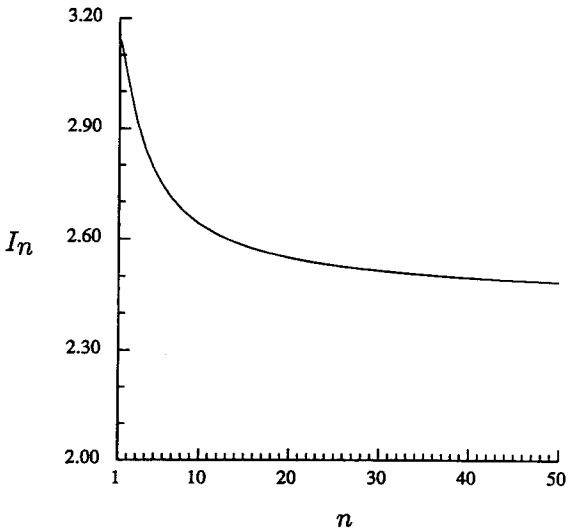

Fig. 4. Variation of I_n with the hardening exponent n.

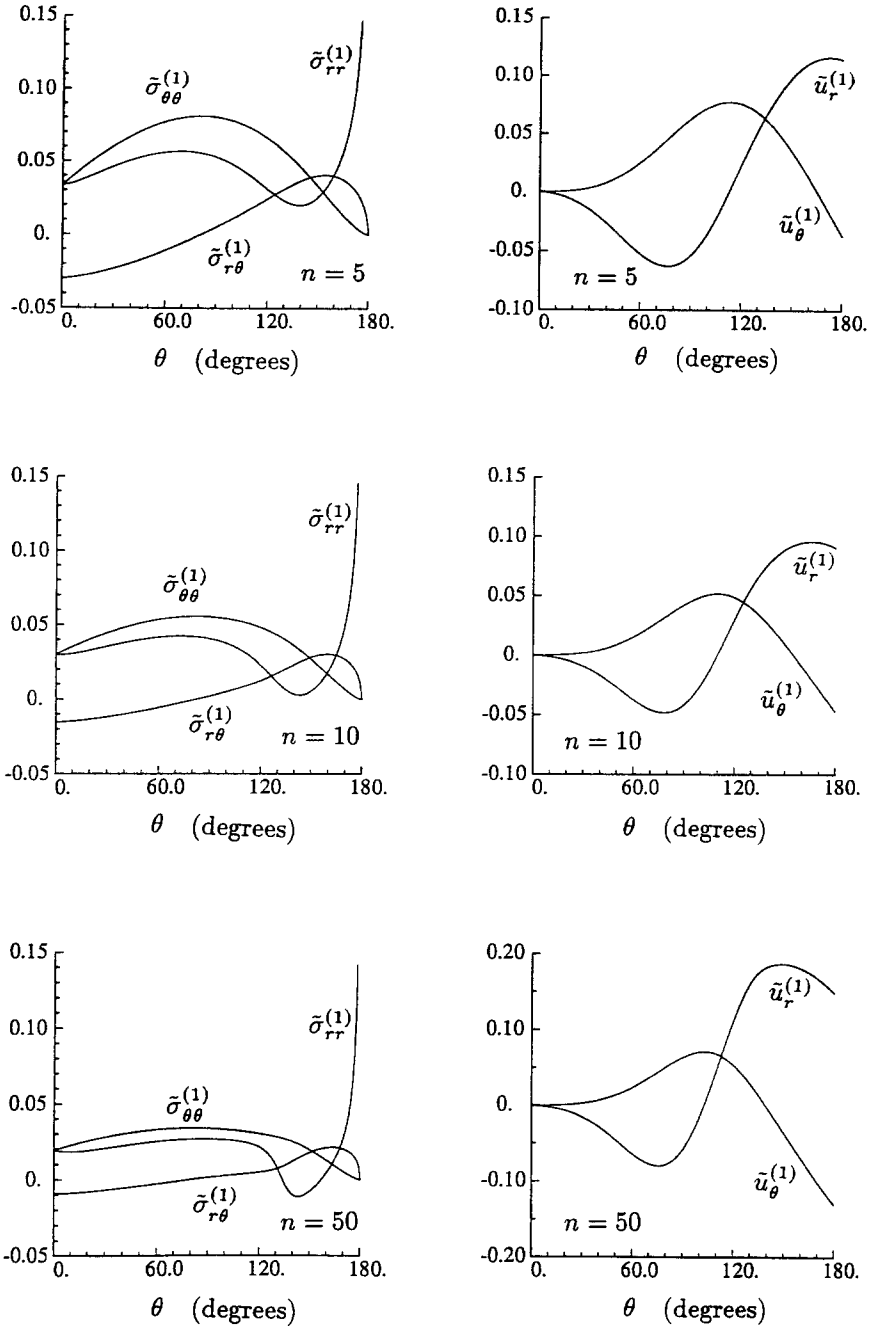

Fig. 5. Angular variation of the second order in-plane stress and displacement components for $n = 5$, 10 and 50.

respectively. A detailed discussion of this topic is given in the following section, where the nature of the asymptotic solution is analysed in detail for values of n near $n = 1$.

Summarizing, we mention that the mathematical limit of the ratio $(\sigma_{\theta\theta}/\sigma_{r\theta})_{\theta=0}$ as $r \to 0$ is completely defined by the hardening exponent n. It is important to realize, however, that for small (but finite) values of r, the second term in the stress expansion becomes important and does affect the near tip mode-mix. Put in other words, for all practical cases, the value of the ratio $(\sigma_{\theta\theta}/\sigma_{r\theta})_{\theta=0}$ near the crack tip depends on both J and Q, which (J, Q) depend, in turn, on the geometry under consideration and the type of applied loading.

It should be also noted that for the two extreme cases of linear elasticity ($n = 1$) and perfect plasticity ($n = \infty$) the stress exponents s and t are equal, i.e.

Table 1.

n	t
2	−0.312
3	−0.212
4	−0.152
5	−0.113
6	−0.087
7	−0.068
8	−0.055
9	−0.045
10	−0.037
11	−0.031
12	−0.026
13	−0.022
14	−0.019
15	−0.016
16	−0.012
17	−0.012
18	−0.011
19	−0.009
20	−0.008

$$s = t = -1/2 \quad \text{for} \quad n = 1, \tag{16}$$

$$s = t = 0 \quad \text{for} \quad n = \infty. \tag{17}$$

This finding is consistent with the known linear elastic solution and the families of slip line fields of Quanxin Guo and Keer (1990) which admit an arbitrary mode-mix at the crack tip.

We conclude this section by mentioning that the asymptotic stress expansion (11) implies the following definition for Q:

$$B_{ij}(r,\theta) = \frac{\sigma_{ij}(r,\theta)/\sigma_0 - [J/(\alpha\epsilon_0\sigma_0 I_n r)]^{1/(n+1)}\tilde{\sigma}_{ij}^{(0)}(\theta)}{[r/(J/\sigma_0)]^t \tilde{\sigma}_{ij}^{(1)}(\theta)}, \tag{18}$$

$$\lim_{r\to 0} B_{ij} = Q = \text{constant} \quad \text{for all } i,j \text{ and } \theta. \tag{19}$$

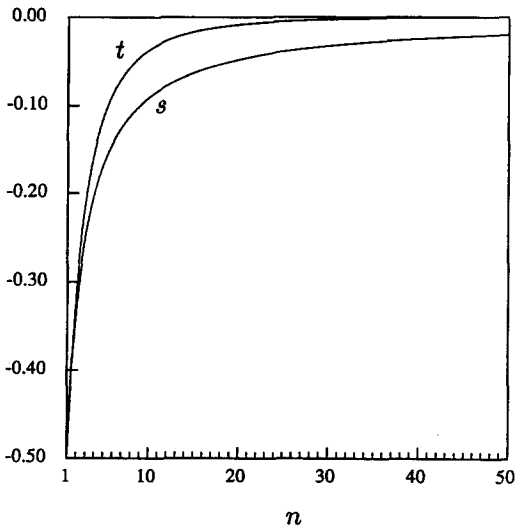

Fig. 6. Variation of the stress exponents s and t with the hardening exponent n.

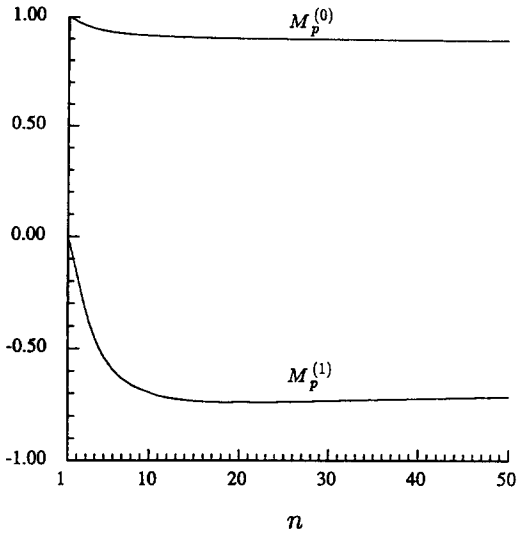

Fig. 7. Variation of the mode-mix parameter M_p with the hardening exponent n.

The predictions of the developed asymptotic solutions are compared with the results of detailed finite element calculations in Section 5.

4. ASYMPTOTIC SOLUTION VIA A PERTURBATION OF n ABOUT $n = 1$

In this section we discuss the behavior of the asymptotic solution near $n = 1$.

The angular functions $\tilde{\mathbf{u}}^{(0)}$, $\tilde{\boldsymbol{\sigma}}^{(0)}$, $\tilde{\mathbf{u}}^{(1)}$ and $\tilde{\boldsymbol{\sigma}}^{(1)}$ introduced in eqns (11) and (12) above, are determined from the solution of the following two eigenvalue problems (Sharma and Aravas, 1991a).

For the leading-order problem we have

$$(s+1)\tilde{\sigma}_{rr}^{(0)} - \tilde{\sigma}_{\theta\theta}^{(0)} + \frac{\mathrm{d}\tilde{\sigma}_{r\theta}^{(0)}}{\mathrm{d}\theta} = 0, \tag{20}$$

$$\frac{\mathrm{d}\tilde{\sigma}_{\theta\theta}^{(0)}}{\mathrm{d}\theta} + (s+2)\tilde{\sigma}_{r\theta}^{(0)} = 0, \tag{21}$$

$$(sn+1)\tilde{u}_r^{(0)} - \tfrac{3}{2}\tilde{\sigma}_e^{(0)n-1}\tilde{s}_{rr}^{(0)} = 0, \tag{22}$$

$$\tilde{u}_r^{(0)} + \frac{\mathrm{d}\tilde{u}_\theta^{(0)}}{\mathrm{d}\theta} - \tfrac{3}{2}\tilde{\sigma}_e^{(0)n-1}\tilde{s}_{\theta\theta}^{(0)} = 0, \tag{23}$$

$$\frac{1}{2}\left(\frac{\mathrm{d}\tilde{u}_r^{(0)}}{\mathrm{d}\theta} + sn\tilde{u}_\theta^{(0)}\right) - \tfrac{3}{2}\tilde{\sigma}_e^{(0)n-1}\tilde{\sigma}_{r\theta}^{(0)} = 0, \tag{24}$$

with boundary conditions

$$\tilde{u}_r^{(0)}(0) = \tilde{u}_\theta^{(0)}(0) = 0, \tag{25}$$

and

$$\tilde{\sigma}_{\theta\theta}^{(0)}(\pi) = \tilde{\sigma}_{r\theta}^{(0)}(\pi) = 0. \tag{26}$$

For next order, the problem is given by

$$(t+1)\tilde{\sigma}_{rr}^{(1)} - \tilde{\sigma}_{\theta\theta}^{(1)} + \frac{\mathrm{d}\tilde{\sigma}_{r\theta}^{(1)}}{\mathrm{d}\theta} = 0, \tag{27}$$

$$\frac{\mathrm{d}\tilde{\sigma}_{\theta\theta}^{(1)}}{\mathrm{d}\theta} + (t+2)\tilde{\sigma}_{r\theta}^{(1)} = 0, \tag{28}$$

$$[s(n-1)+t+1]\tilde{u}_r^{(1)} - \tfrac{3}{2}\tilde{\sigma}_e^{(0)n-1}\left[\tilde{s}_{rr}^{(1)} + \tfrac{3}{2}(n-1)\frac{\tilde{s}_{kl}^{(0)}\tilde{\sigma}_{kl}^{(1)}}{\tilde{\sigma}_e^{(0)2}}\tilde{s}_{rr}^{(0)}\right] = 0, \tag{29}$$

$$\tilde{u}_r^{(1)} + \frac{\mathrm{d}\tilde{u}_\theta^{(1)}}{\mathrm{d}\theta} - \tfrac{3}{2}\tilde{\sigma}_e^{(0)n-1}\left[\tilde{s}_{\theta\theta}^{(1)} + \tfrac{3}{2}(n-1)\frac{\tilde{s}_{kl}^{(0)}\tilde{\sigma}_{kl}^{(1)}}{\tilde{\sigma}_e^{(0)2}}s_{\theta\theta}^{(0)}\right] = 0, \tag{30}$$

$$\frac{1}{2}\left[\frac{\mathrm{d}\tilde{u}_r^{(1)}}{\mathrm{d}\theta} + (s(n-1)+t)\tilde{u}_\theta^{(1)}\right] - \tfrac{3}{2}\tilde{\sigma}_e^{(0)n-1}\left[\tilde{\sigma}_{r\theta}^{(1)} + \tfrac{3}{2}(n-1)\frac{\tilde{s}_{kl}^{(0)}\tilde{\sigma}_{kl}^{(1)}}{\tilde{\sigma}_e^{(0)2}}\tilde{\sigma}_{r\theta}^{(0)}\right] = 0, \tag{31}$$

with boundary conditions

$$\tilde{u}_r^{(1)}(0) = \tilde{u}_\theta^{(1)}(0) = 0, \tag{32}$$

and

$$\tilde{\sigma}_{\theta\theta}^{(1)}(\pi) = \tilde{\sigma}_{r\theta}^{(1)}(\pi) = 0. \tag{33}$$

The only out-of-plane non-zero stress component σ_{zz} is determined from the plane strain condition $\epsilon_{zz} = 0$, which implies that $\tilde{\sigma}_{zz}^{(0)} = (\tilde{\sigma}_{rr}^{(0)} + \tilde{\sigma}_{\theta\theta}^{(0)})/2$ and $\tilde{\sigma}_{zz}^{(1)} = (\tilde{\sigma}_{rr}^{(1)} + \tilde{\sigma}_{\theta\theta}^{(1)})/2$.

An obvious solution to the second-order eigenvalue problem (27)–(33) is

$$t = s, \quad \tilde{\mathbf{u}}^{(1)} = c\tilde{\mathbf{u}}^{(0)}, \quad \tilde{\boldsymbol{\sigma}}^{(1)} = c\tilde{\boldsymbol{\sigma}}^{(0)}/n, \tag{34}$$

where c is an arbitrary constant. This solution, however, is not acceptable, since it violates the condition $s < t$.

In the following, we study the plane strain version of the two eigenvalue problems given above, near $n = 1$. Such an analysis for the leading-order problem (20)–(26) has been presented by Champion and Atkinson (1991) who formulated the problem in terms of a displacement potential. The solution presented in Section 4.1 parallels that of Champion and Atkinson and is used in Section 4.2 for the analysis of the second-order problem (27)–(33).

4.1. *The leading-order problem*

Substituting $n = 1+\epsilon$ in eqns (20)–(24) and expanding in ϵ, we find

$$\frac{\mathrm{d}\mathbf{x}(\theta)}{\mathrm{d}\theta} - \mathbf{F}(s)\cdot\mathbf{x}(\theta) = \epsilon\mathbf{G}(\mathbf{x}, s)\cdot\mathbf{x}(\theta), \tag{35}$$

where

$$\mathbf{x} = \{\tilde{u}_r^{(0)}, \tilde{u}_\theta^{(0)}, \tilde{\sigma}_{\theta\theta}^{(0)}, \tilde{\sigma}_{r\theta}^{(0)}\}, \tag{36}$$

$$\mathbf{G} = \mathbf{G}^{(0)} + O(\varepsilon), \tag{37}$$

and $(\mathbf{F}, \mathbf{G}^{(0)})$ are two 4×4 matrices which are given in Appendix A. The $\tilde{\sigma}_{rr}^{(0)}$ stress component, which is not included in $\mathbf{x}$, is determined from the algebraic equation (22).

Equation (35) can be rewritten in an integral equation form as

$$\mathbf{x}(\theta) = \mathbf{\Psi}(\theta, s) \cdot \mathbf{\Psi}^{-1}(0, s) \cdot \mathbf{x}(0) + \epsilon \mathbf{\Psi}(\theta, s) \cdot \int_0^\theta \mathbf{\Psi}(\phi, s) \cdot \mathbf{G}(\mathbf{x}(\phi), s) \cdot \mathbf{x}(\phi)\, \mathrm{d}\phi, \tag{38}$$

where $\mathbf{\Psi}$ is a 4×4 matrix defined in Appendix A.

We let $\mathbf{x}(0) = \{0, 0, A_{\mathrm{I}}, A_{\mathrm{II}}\}$, so that the boundary conditions on $\theta = 0$ [eqns (25)] are satisfied automatically.

We attempt an asymptotic expansion of the solution in the form

$$\mathbf{x}(\theta) = \mathbf{x}^{(0)}(\theta) + \epsilon \mathbf{x}^{(1)}(\theta) + O(\epsilon^2). \tag{39}$$

Substituting the expansion (39) together with

$$s = -\frac{1}{n+1} = -\tfrac{1}{2} + \tfrac{1}{4}\epsilon - \tfrac{1}{8}\epsilon^2 + O(\epsilon^3), \tag{40}$$

into (38) and collecting terms having like powers of ϵ, we find

$$\mathbf{x}^{(0)}(\theta) = \mathbf{\Psi}(\theta, -\tfrac{1}{2}) \cdot \mathbf{\Psi}^{-1}(0, -\tfrac{1}{2}) \cdot \mathbf{x}(0), \tag{41}$$

$$\mathbf{x}^{(1)}(\theta) = \frac{1}{4} \frac{\partial}{\partial s} [\mathbf{\Psi}(\theta, s) \cdot \mathbf{\Psi}^{-1}(0, s)]_{s=-1/2} \cdot \mathbf{x}(0) + \mathbf{\Psi}(\theta, -\tfrac{1}{2}) \cdot \int_0^\theta \mathbf{\Psi}^{-1}(\phi, -\tfrac{1}{2}) \cdot \mathbf{G}^{(0)}(\mathbf{x}^{(0)}(\phi), -\tfrac{1}{2}) \cdot \mathbf{x}^{(0)}(\phi)\, \mathrm{d}\phi. \tag{42}$$

The functions $\mathbf{x}^{(0)}(\theta)$ and $\mathbf{x}^{(1)}(\theta)$ are evaluated using *Mathematica* (Wolfram, 1991). The leading order solution $\mathbf{x}^{(0)}(\theta)$ ($\varepsilon = 0$, $n = 1$) is of the form (see Appendix A)

$$\mathbf{x}^{(0)}(\theta) = A_{\mathrm{I}} \mathbf{x}_{\mathrm{I}}(\theta) + A_{\mathrm{II}} \mathbf{x}_{\mathrm{II}}(\theta), \tag{43}$$

and corresponds to an incompressible linear elastic material, where A_{I} and A_{II} are arbitrary constants, and $\mathbf{x}_{\mathrm{I}}(\theta)$ and $\mathbf{x}_{\mathrm{II}}(\theta)$ are the standard mode-I and mode-II solutions, respectively.

Next, we consider the remaining boundary conditions on $\theta = \pi$ [eqns (26)]. It can be readily shown that the boundary conditions (26) are automatically satisfied to $O(1)$, i.e. $x_3^{(0)}(\pi) = x_4^{(0)}(\pi) = 0$ for all A_{I} and A_{II}. Satisfaction of (26) to order ϵ requires that

$$x_3^{(1)}(\pi) = x_4^{(1)}(\pi) = 0, \tag{44}$$

which leads to

$$-4 \frac{A_{\mathrm{II}}}{A_{\mathrm{I}}} + 3 I_1\left(\frac{A_{\mathrm{II}}}{A_{\mathrm{I}}}\right) = 0, \tag{45}$$

$$8 + 3 I_2\left(\frac{A_{\mathrm{II}}}{A_{\mathrm{I}}}\right) = 0, \tag{46}$$

where the functions I_1 and I_2 are defined in Appendix A. The last two equations are solved numerically for $A_{\mathrm{II}}/A_{\mathrm{I}}$. It is found that they have the common solution $A_{\mathrm{II}}/A_{\mathrm{I}} = 0$. Equation (43) reduces now to $\mathbf{x}^{(0)}(\theta) = A_{\mathrm{I}} \mathbf{x}_{\mathrm{I}}(\theta)$, i.e. the leading order solution branches from the mode-I linear elastic solution.

4.2. *The second-order problem*

Substituting $n = 1 + \epsilon$ and $\mathbf{x}(\theta) = \mathbf{x}^{(0)}(\theta) + \epsilon \mathbf{x}^{(1)}(\theta) + O(\epsilon^2)$ into eqns (27)–(31) and expanding in ϵ, we find

$$\frac{\mathrm{d}\mathbf{y}(\theta)}{\mathrm{d}\theta} - \mathbf{F}(t)\cdot\mathbf{y}(\theta) = \epsilon\hat{\mathbf{G}}(\theta,t)\cdot\mathbf{y}(\theta), \tag{47}$$

where

$$\mathbf{y} = \{\tilde{u}_r^{(1)}, \tilde{u}_\theta^{(1)}, \tilde{\sigma}_{\theta\theta}^{(1)}, \tilde{\sigma}_{r\theta}^{(1)}\}, \tag{48}$$

$$\hat{\mathbf{G}} = \hat{\mathbf{G}}^{(0)} + \epsilon\hat{\mathbf{G}}^{(1)} + O(\epsilon^2), \tag{49}$$

$\mathbf{F}$ is the matrix defined in Section 4.1, and $(\hat{\mathbf{G}}^{(0)}, \hat{\mathbf{G}}^{(1)})$ are two 4×4 matrices which are given in Appendix B. The $\tilde{\sigma}_{rr}^{(1)}$ stress component, which is not included in $\mathbf{y}$, is determined from the algebraic equation (29).

Equation (47) can be written in the form:

$$\mathbf{y}(\theta) = \mathbf{\Psi}(\theta,t)\cdot\mathbf{\Psi}^{-1}(0,t)\cdot\mathbf{y}(0) + \epsilon\mathbf{\Psi}(\theta,t)\cdot\int_0^\theta \mathbf{\Psi}(\phi,t)\cdot\hat{\mathbf{G}}(\phi,t)\cdot\mathbf{y}(\phi)\,\mathrm{d}\phi, \tag{50}$$

where $\mathbf{\Psi}$ is the matrix introduced in Section 4.1.

We write $\mathbf{y}(0) = \{0, 0, B_{\mathrm{I}}, B_{\mathrm{II}}\}$, so that the boundary conditions on $\theta = 0$ are satisfied automatically.

We attempt an asymptotic expansion of the solution in the form

$$\mathbf{y}(\theta) = \mathbf{y}^{(0)}(\theta) + \epsilon\mathbf{y}^{(1)}(\theta) + \epsilon^2\mathbf{y}^{(2)}(\theta) + O(\epsilon^3), \tag{51}$$

and

$$t = -\tfrac{1}{2} + \epsilon C + \epsilon^2 D + O(\epsilon^3), \tag{52}$$

where C and D are constants to be determined.

Substituting the expansions (51), (52), (49) and (40) into (50) and collecting terms having like powers of ε, we find

$$\mathbf{y}^{(0)}(\theta) = \mathbf{\Psi}(\theta, -\tfrac{1}{2})\cdot\mathbf{\Psi}^{-1}(0, -\tfrac{1}{2})\cdot\mathbf{y}(0), \tag{53}$$

$$\mathbf{y}^{(1)}(\theta) = \left\{C\frac{\partial}{\partial t}[\mathbf{\Psi}(\theta,t)\cdot\mathbf{\Psi}^{-1}(0,t)]\right\}_{t=-1/2}\cdot\mathbf{y}(0) + \mathbf{\Psi}(\theta,-\tfrac{1}{2})\cdot\int_0^\theta \mathbf{\Psi}^{-1}(\phi,-\tfrac{1}{2})\cdot\hat{\mathbf{G}}^{(0)}(\phi,-\tfrac{1}{2})\cdot\mathbf{y}^{(0)}(\phi)\,\mathrm{d}\phi, \tag{54}$$

$$\mathbf{y}^{(2)}(\theta) = \left\{D\frac{\partial}{\partial t}[\mathbf{\Psi}(\theta,t)\cdot\mathbf{\Psi}^{-1}(0,t)] + \tfrac{1}{2}C^2\frac{\partial^2}{\partial t^2}[\mathbf{\Psi}(\theta,t)\cdot\mathbf{\Psi}^{-1}(0,t)]\right\}_{t=-1/2}\cdot\mathbf{y}(0) + C\left\{\frac{\partial}{\partial t}\left[\mathbf{\Psi}(\theta,t)\cdot\int_0^\theta \mathbf{\Psi}^{-1}(\phi,t)\cdot\hat{\mathbf{G}}^{(0)}(\phi,t)\cdot\mathbf{y}^{(0)}(\phi)\,\mathrm{d}\phi\right]\right\}_{t=-1/2} + \mathbf{\Psi}(\theta,-\tfrac{1}{2})\cdot\int_0^\theta \mathbf{\Psi}^{-1}(\phi,-\tfrac{1}{2})\cdot[\hat{\mathbf{G}}^{(0)}(\phi,-\tfrac{1}{2})\cdot\mathbf{y}^{(1)}(\phi) + \hat{\mathbf{G}}^{(1)}(\phi,-\tfrac{1}{2})\cdot\mathbf{y}^{(0)}(\phi)]\,\mathrm{d}\phi. \tag{55}$$

Again, $\mathbf{y}^{(0)}(\theta)$ and $\mathbf{y}^{(1)}(\theta)$ are evaluated using *Mathematica* and are used for the determination of $\mathbf{y}^{(2)}(\theta)$ (see Appendix B). The leading order solution $\mathbf{y}^{(0)}(\theta)$ ($\epsilon = 0$, $n = 1$) is of the form

$$\mathbf{y}^{(0)}(\theta) = B_{\mathrm{I}}\mathbf{x}_{\mathrm{I}}(\theta) + B_{\mathrm{II}}\mathbf{x}_{\mathrm{II}}(\theta), \tag{56}$$

where B_{I} and B_{II} are arbitrary constants, and $\mathbf{x}_{\mathrm{I}}(\theta)$ and $\mathbf{x}_{\mathrm{II}}(\theta)$ are the standard mode-I and mode-II functions introduced in Section 4.1.

We consider next the remaining boundary conditions on $\theta = \pi$ [eqns (26)]. The boundary conditions (26) are automatically satisfied to $O(1)$. Satisfaction of (26) to order ϵ and ϵ^2 requires that

$$y_3^{(1)}(\pi) = y_4^{(1)}(\pi) = 0 \tag{57}$$

and

$$y_3^{(2)}(\pi) = y_4^{(2)}(\pi) = 0. \tag{58}$$

Using *Mathematica*, we can readily show that (57) and (54) lead to

$$B_{\mathrm{I}}(C - \tfrac{1}{4}) = 0 \quad \text{and} \quad B_{\mathrm{II}}(C - \tfrac{1}{4}) = 0, \tag{59}$$

with the only non-trivial solution

$$C = \tfrac{1}{4}. \tag{60}$$

Similarly, (58) and (55) imply that

$$(D + \tfrac{1}{8})B_{\mathrm{I}} = 0, \tag{61}$$

$$(D + \tfrac{1}{16})B_{\mathrm{II}} = 0. \tag{62}$$

There are two possible solutions to the last two equations:

$$D = -\tfrac{1}{8} \quad \text{and} \quad B_{\mathrm{II}} = 0, \tag{63}$$

and

$$D = -\tfrac{1}{16} \quad \text{and} \quad B_{\mathrm{I}} = 0. \tag{64}$$

The solution (63) corresponds to the obvious solution (34) and must be rejected; therefore, we are left with (64). Equation (56) reduces now to $\mathbf{y}^{(0)}(\theta) = B_{\mathrm{II}}\mathbf{x}_{\mathrm{II}}(\theta)$, i.e. the second order asymptotic solution branches from the mode-II linear elastic solution.

Summarizing, we mention that

$$s = -\frac{1}{n+1} = -\tfrac{1}{2} + \tfrac{1}{4}\epsilon - \tfrac{1}{8}\epsilon^2 + O(\epsilon^3) \quad \text{and} \quad A_{\mathrm{II}} = 0, \tag{65}$$

$$t = -\tfrac{1}{2} + \tfrac{1}{4}\epsilon - \tfrac{1}{16}\epsilon^2 + O(\epsilon^3) \quad \text{and} \quad B_{\mathrm{I}} = 0, \tag{66}$$

i.e. $t = s + O(\epsilon^2)$ near $n = 1$, and $\tilde{\boldsymbol{\sigma}}^{(0)}$, $\tilde{\boldsymbol{\sigma}}^{(1)}$ on the right-hand side of (11) branch from the mode-I and mode-II linear elastic solutions respectively.

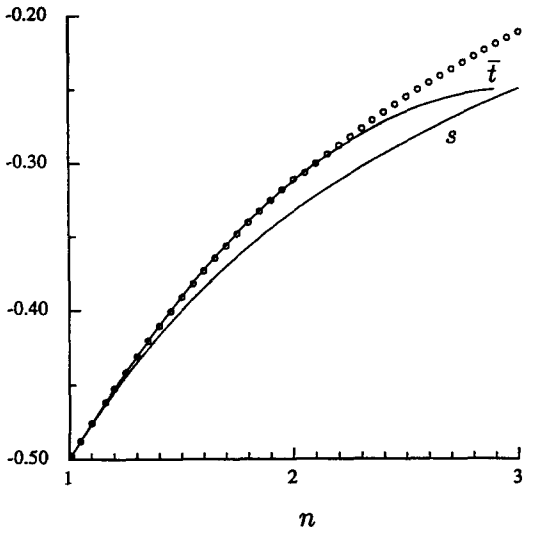

Fig. 8. Variation of s and t near $n = 1$. $\bar{t}$ is given by eqn (66).

Figure 8 shows the variation of s and t near $n = 1$. The open circles in that figure are the results of the numerical solution of the eigenvalue problem (27)–(33), and the curve marked $\bar{t}$ is the variation of t as predicted by the asymptotic solution above to within terms of $O(\epsilon^3)$, i.e. $\bar{t} = -1/2+\epsilon/4-\epsilon^2/16$ [see (66) above]. The predictions of the asymptotic solution (66) agree very well with the results of the numerical solution in the region $1 \leqslant n \leqslant 2$.

We conclude this section by mentioning that the corresponding linear elastic asymptotic solution is written in terms of the complex stress intensity factor $K = K_1 + iK_2 = |K| e^{i\phi}$, and the near-tip stresses can be characterized by the two scalar quantities K_1 and K_2 (or $|K|$ and ϕ). Therefore, J and Q in the asymptotic expansion (11) can be viewed as the non-linear counterparts of K_1 and K_2 (or $|K|$ and ϕ).

5. THE LINEAR ELASTIC SUBSTRATE

In this section, we show that the two-term asymptotic solution developed in Section 3 is still valid when the rigid substrate is replaced by a linear elastic material which is perfectly bonded to the non-linear material (Fig. 9).

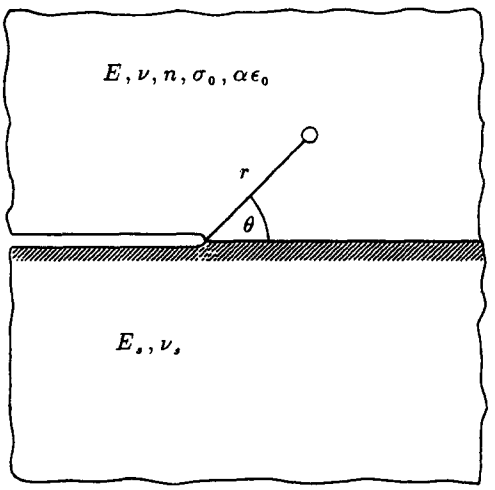

Fig. 9. Crack along the interface between a power-law hardening material and a linear elastic substrate.

Referring to Fig. 9, we write the boundary conditions for the asymptotic problem as

$$\sigma_{\theta\theta} = \sigma_{r\theta} = 0 \quad \text{on} \quad \theta = \pm\pi. \tag{67}$$

The continuity conditions along the interface are

$$[\sigma_{\theta\theta}] = [\sigma_{r\theta}] = 0, \quad [\mathbf{u}] = \mathbf{0} \quad \text{on} \quad \theta = 0, \tag{68}$$

where [ ] denotes jumps of the functions across the interface.

We assume that the near tip stress expansion is of the form

$$\boldsymbol{\sigma}(r,\theta) = r^s\boldsymbol{\sigma}^{(0)}(\theta) + r^t\boldsymbol{\sigma}^{(1)}(\theta) + \cdots, \quad -\pi \leqslant \theta \leqslant \pi, \quad \text{as} \quad r \to 0, \tag{69}$$

where $s = -1/(n+1)$, and $s < t < \cdots$.

The corresponding form of the near tip displacement field is

$$\mathbf{u}(r,\theta) = r^{sn+1}\mathbf{u}^{(0)}(\theta) + r^{s(n-1)+t+1}\mathbf{u}^{(1)}(\theta) + \cdots, \quad 0 \leqslant \theta \leqslant \pi, \quad \text{as} \quad r \to 0, \tag{70}$$

$$\mathbf{u}(r,\theta) = r^{s+1}\hat{\mathbf{u}}^{(0)}(\theta) + r^{t+1}\hat{\mathbf{u}}^{(1)}(\theta) + \cdots, \quad -\pi \leqslant \theta \leqslant 0, \quad \text{as} \quad r \to 0, \tag{71}$$

provided that $t < (n-2)/(n+1)$ (Sharma and Aravas, 1991a).

The displacement continuity condition (68b) now becomes

$$[r^{sn+1}\mathbf{u}^{(0)}(0) + r^{s(n-1)+t+1}\mathbf{u}^{(1)}(0) + \cdots] - [r^{s+1}\hat{\mathbf{u}}^{(0)}(0) + \cdots] = \mathbf{0} \quad \text{as} \quad r \to 0. \tag{72}$$

Taking into account that $s = -1/(n+1)$ and $t < (n-2)/(n+1)$, we conclude that, to leading and second order, the displacement continuity condition (72) implies that

$$\mathbf{u}^{(0)}(0) = \mathbf{u}^{(1)}(0) = \mathbf{0}. \tag{73}$$

Summarizing, we mention that the asymptotic boundary conditions in the region $0 \leqslant \theta \leqslant \pi$ are

$$\sigma^{(0)}_{\theta\theta}(\pi) = \sigma^{(0)}_{r\theta}(\pi) = 0, \quad \mathbf{u}^{(0)}(0) = \mathbf{0}, \tag{74}$$

and

$$\sigma^{(1)}_{\theta\theta}(\pi) = \sigma^{(1)}_{r\theta}(\pi) = 0, \quad \mathbf{u}^{(1)}(0) = \mathbf{0}, \tag{75}$$

which shows that the two-term asymptotic solution developed in Section 3 is still valid in the region $0 \leqslant \theta \leqslant \pi$, i.e. the effects of the linear elastic substrate enter the asymptotic solution in the non-linear material to third order or higher.

Next, we briefly discuss the case in which the substrate is made of a power-law hardening material with a hardening exponent $n_s < n$. In that case, using the results of Sharma and Aravas (1991b), we can readily conclude that the two-term asymptotic solution developed in Section 3 is still valid in the region $0 \leqslant \theta \leqslant \pi$, provided that

$$n_s < n - 1 - t(n+1), \tag{76}$$

where the value of t is given in terms of n in Table 1.

6. FINITE ELEMENT SOLUTIONS

In order to verify the asymptotic solutions developed in the previous sections, we carry out finite element calculations under small- as well as large-scale yielding conditions.

The finite element model is constructed using 9-node isoparametric elements with 3×3 Gauss integration. To avoid numerical difficulties, which arise from the nearly incompressible deformation of the material, the so-called B-bar method is used (Hughes, 1980, 1987), i.e. the deviatoric part of the strain tensor is calculated at the 3×3 Gauss points whereas the volumetric part is evaluated at the 2×2 Gauss points and then interpolated/extrapolated to the 3×3 Gauss points.

Infinitesimal strains are assumed in the calculations.

The ABAQUS general purpose finite element program (Hibbitt, 1984) is used for the computations. It should be mentioned that the 9-node element is not included in the ABAQUS "element library"; however, the code provides a general interface so that a new element can be introduced as a "user subroutine". The constitutive behavior is part of the element definition.

6.1. *Small scale yielding deformation plasticity solutions*

We consider the crack-tip region of a plane strain crack lying along the interface of an elastoplastic medium and a rigid substrate and use a boundary layer formulation to study the near-tip elastoplastic fields. The linear elastic asymptotic displacement field is applied on a semicircular boundary remote from the tip. Perfect bonding is assumed ahead of the crack and the crack face is kept traction-free. A semi-circular arrangement of wedge-shaped (collapsed) elements is used around the crack tip and all crack-tip nodes are tied together. The deformation plasticity model discussed in Section 3 was implemented through the user interface. The material constants used in the calculations are $E/\sigma_0 = 300$, $\nu = 0.3$, $n = 5$ and $\alpha = 1$. The radial length of each of the wedge-shaped elements is 10^{-10} times the outermost radius of the finite element mesh.

Dimensional analysis shows that the solution of the problem must be of the form (Shih and Asaro, 1989)

$$\boldsymbol{\sigma} = \sigma_0 \mathbf{F}\left(\frac{r}{K\bar{K}/\sigma_0^2}, \theta, \xi, \frac{E}{\sigma_0}, \nu, n, \alpha\right), \tag{77}$$

where $\mathbf{F}$ is a dimensionless tensor-valued function, K is the complex stress intensity factor (Rice, 1988), the overbar denotes complex conjugate,

$$\xi = \varphi + \varepsilon \ln\left(\frac{K\bar{K}}{\sigma_0^2}\right), \tag{78}$$

φ is the phase angle of K, and $\varepsilon = [1/(2\pi)] \ln(3-4\nu)$. The function $\mathbf{F}$ has a periodicity with respect to ξ of the form (Shih and Asaro, 1989)

$$\mathbf{F}(\xi + m\pi) = (-1)^m \mathbf{F}(\xi), \quad m = \text{integer}. \tag{79}$$

In order to obtain a better understanding of the nature of the parameter ξ, we make a connection with a problem of a plane strain Griffith crack of length $2a$ loaded as shown in Fig. 10. In that case (Rice, 1988)

$$K = |K| e^{i\varphi}, \quad |K| = T\sqrt{\pi a}\sqrt{1+4\varepsilon^2}, \quad \varphi = \psi + \beta - \varepsilon \ln(2a), \tag{80}$$

where $\beta = \tan^{-1}(2\varepsilon)$, ψ is the far-field loading angle as shown in Fig. 10, and T is the magnitude of the applied traction at infinity. The ξ-parameter now becomes

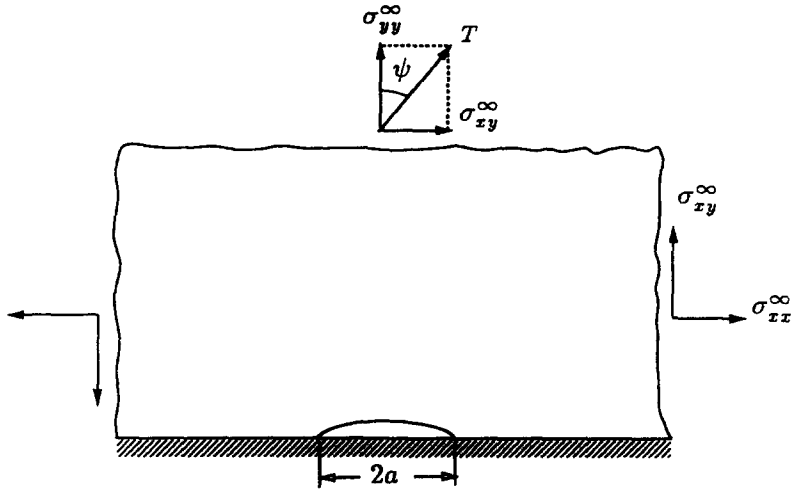

Fig. 10. Griffith crack at the interface of a deformable medium and a rigid substrate.

$$\xi = \psi + \beta + \varepsilon \ln\left[(1+4\varepsilon^2)\frac{\pi}{2}\left(\frac{T}{\sigma_0}\right)^2\right]. \tag{81}$$

In view of the above definition of ξ and the periodicity (79), the stresses for $\psi = -90°$ are the opposite of those for $\psi = 90°$ at the same load level under small scale yielding conditions.

For the case of the Griffith crack and for applied tractions T/σ_0 in the range 10^{-2}–10^{-1} (small scale yielding) the corresponding values of ξ are

$$\xi = -1.417 \quad \text{to} \quad -0.986 \quad \text{for} \quad \psi = -45°,$$
$$\xi = -0.631 \quad \text{to} \quad -0.200 \quad \text{for} \quad \psi = 0°,$$
$$\xi = -0.154 \quad \text{to} \quad 0.585 \quad \text{for} \quad \psi = 45°,$$

and

$$\xi = 0.940 \quad \text{to} \quad 1.370 \quad \text{for} \quad \psi = 90°.$$

The stress intensity factor used in the boundary conditions of the finite element calculations is determined using eqn (80), so that connection with the Griffith crack problem can be made. Four sets of calculations were carried out, with values of $\psi = 0°$, $\pm 45°$, and $90°$; in all cases, the calculations were terminated at the load level $T/\sigma_0 = 0.222$. At the end of the calculations, the maximum extent of the plastic zone, which is defined as the region where $\sigma_e \geqslant \sigma_0$, is of order $10^{-2}R_{out}$, where R_{out} is the outermost radius of the finite element mesh.

All results presented in the following are for the final load level $T/\sigma_0 = 0.222$. At this load level and for loading angles $\psi = -45°$, $0°$, $45°$, $90°$ the values of ξ are $\xi = -0.837$, -0.051, 0.734, 1.519 respectively.

Figure 11 shows the angular variation of the normalized in-plane stress components for the four cases analysed at the radial distance $r = 1.1 \times 10^{-7} K\bar{K}/\sigma_0^2$. In Fig. 11, and in all subsequent figures, the open circles indicate the results of the finite element calculations, curve I is the first term in stress expansion (11), and curve II is the sum of the first two terms in (11). The method used for the calculation of the constant Q is discussed later in this section. For the case of $\psi = 0°$ ($\xi = -0.051$) the asymptotic solution agrees well with the finite element solution and inclusion of the second term in (11) does improve the prediction of the asymptotic solution. For the values of $\psi = -45°$, $45°$, and $90°$ ($\xi = -0.837$, 0.734, and 1.519), however, the agreement is not always good, especially in the region ahead of the crack ($0° \leqslant \theta \leqslant 60°$), where higher order terms in the stress expansion (11) appear to have an important contribution. Figure 11 makes it clear that the region

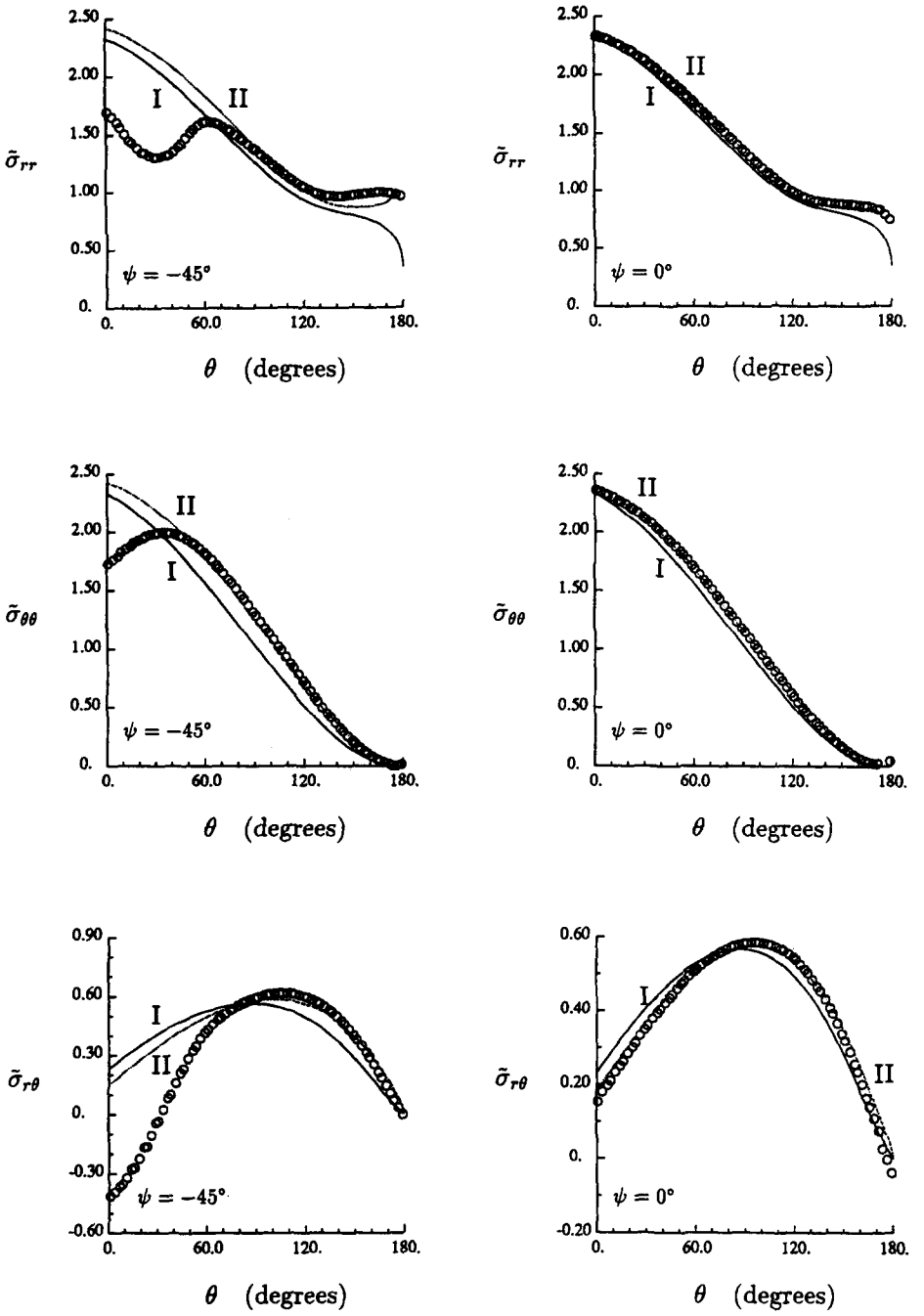

Fig. 11. Angular variation of the normalized in-plane stress components $\tilde{\sigma}_{ij} = \sigma_{ij}/\{J/(\alpha\varepsilon_0 I_n)^{1/(n+1)}\}$ for $\psi = -45°$, 0°, 45° and 90° ($\xi = -0.837$, -0.051, 0.734 and 1.519) at a radial distance $r = 1.1 \times 10^{-7} K\tilde{R}/\sigma_0^2$.

of dominance of the asymptotic solution depends strongly on θ as well as the value of ξ, which depends, in turn, on the geometry considered and the magnitude and direction of the remote loading.

Figure 12 shows the radial variation of the in-plane stress components along the radial line $\theta = 86.25°$ for the four cases analysed. The region of dominance of the asymptotic solution is shown again to be a strong function of the type of remote loading and θ. For example, when $\psi = 0°$ ($\xi = -0.051$), the radial distance over which the difference between the asymptotic and the finite element solution is less than 10% ranges from $0.01 r_{max}^{p}$ along $\theta = 90°$ to $10^{-7} r_{max}^{p}$ along $\theta = 0°$, where r_{max}^{p} is the maximum extent of the plastic zone.

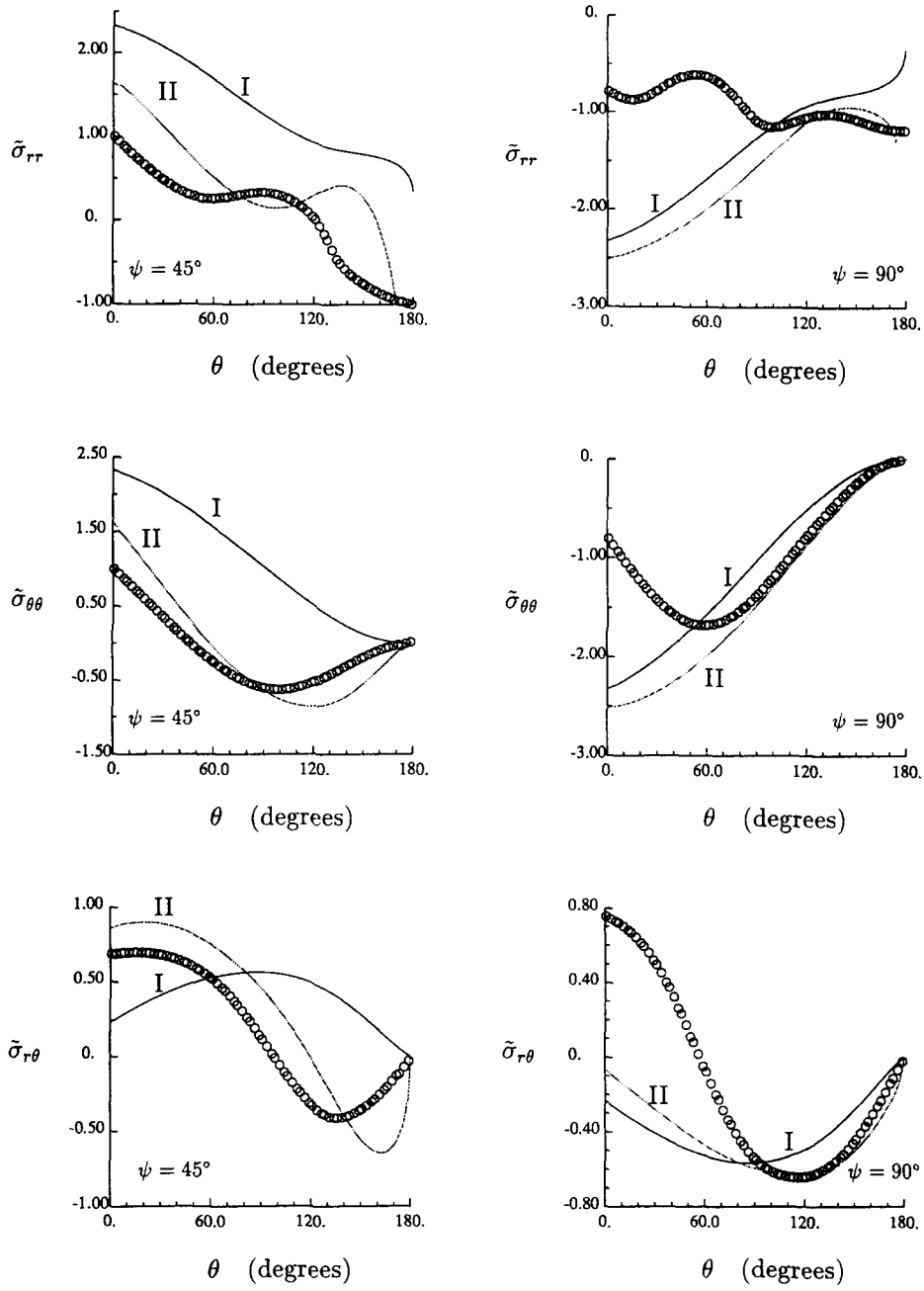

Fig. 11. *Continued.*

The values of Q used in Figs 11 and 12 are determined using eqn (19) together with the finite element solutions. Figure 13 shows the variation of $B_{\theta\theta}$ for different values of θ at the final load level for the four cases analysed. The other two in-plane components B_{rr} and $B_{r\theta}$ show similar variations. According to eqn (19), all B_{ij} components should approach the constant Q value as $r \to 0$. Figure 13 shows that for $\psi = -45°$, $B_{\theta\theta}$ approaches a constant as $r \to 0$ for $\theta > 25°$, which suggests that the region of dominance of the two-term asymptotic solution is vanishingly small in the angular region $0° < \theta < 25°$. For the case of $\psi = 0°$, Q does approach a constant as $r \to 0$ for all values of θ. For $\psi = 45°$, the limit of $B_{\theta\theta}$ as $r \to 0$ depends on θ [see Fig. 13(c)], which shows that the region of dominance shrinks to zero in this case. Finally, when $\psi = 90°$, $B_{\theta\theta}$ approaches a constant value as $r \to 0$ only when $\theta > 85°$, implying that the region of dominance of the two-term asymptotic solution is vanishingly small in the angular region $0° < \theta < 85°$.

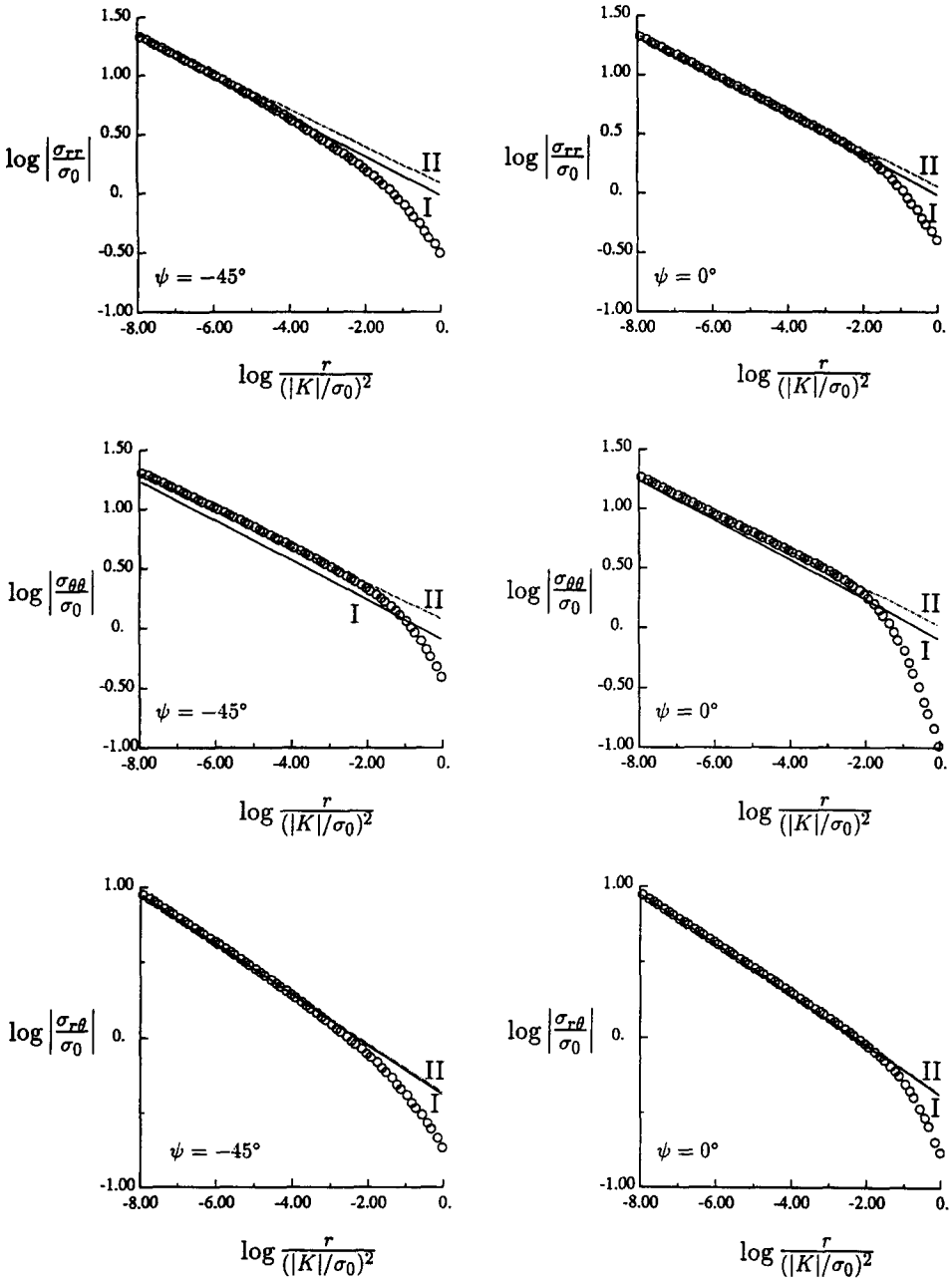

Fig. 12. Radial variation of the normalized in-plane stress components for $\psi = -45°$, 0°, 45° and 90° ($\xi = -0.837$, -0.051, 0.734 and 1.519), along $\theta = 86.25°$.

Notice that for the case of $\psi = 90°$, the finite element solution indicates that the crack face penetrates the rigid substrate, i.e. $u_\theta > 0$ on $\theta = \pi$ near the crack tip. However, the asymptotic solutions presented in Section 3 are normalized so that $\tilde{u}_\theta^{(0)}(\pi) < 0$. Therefore, for the case of $\psi = 90°$, we use the opposite of the asymptotic solution shown in Fig. 2 for $n = 5$.

The values of Q used in Figs 11 and 12 are $Q = 10$, 6, -75 and -18 for $\psi = -45°$, 0°, 45° and 90°, respectively.

6.2. *Large scale yielding flow theory solutions*

We consider a plane strain edge crack of length a along the interface between an elastic–plastic medium and a rigid substrate. A remote tensile load σ^∞ is applied as shown

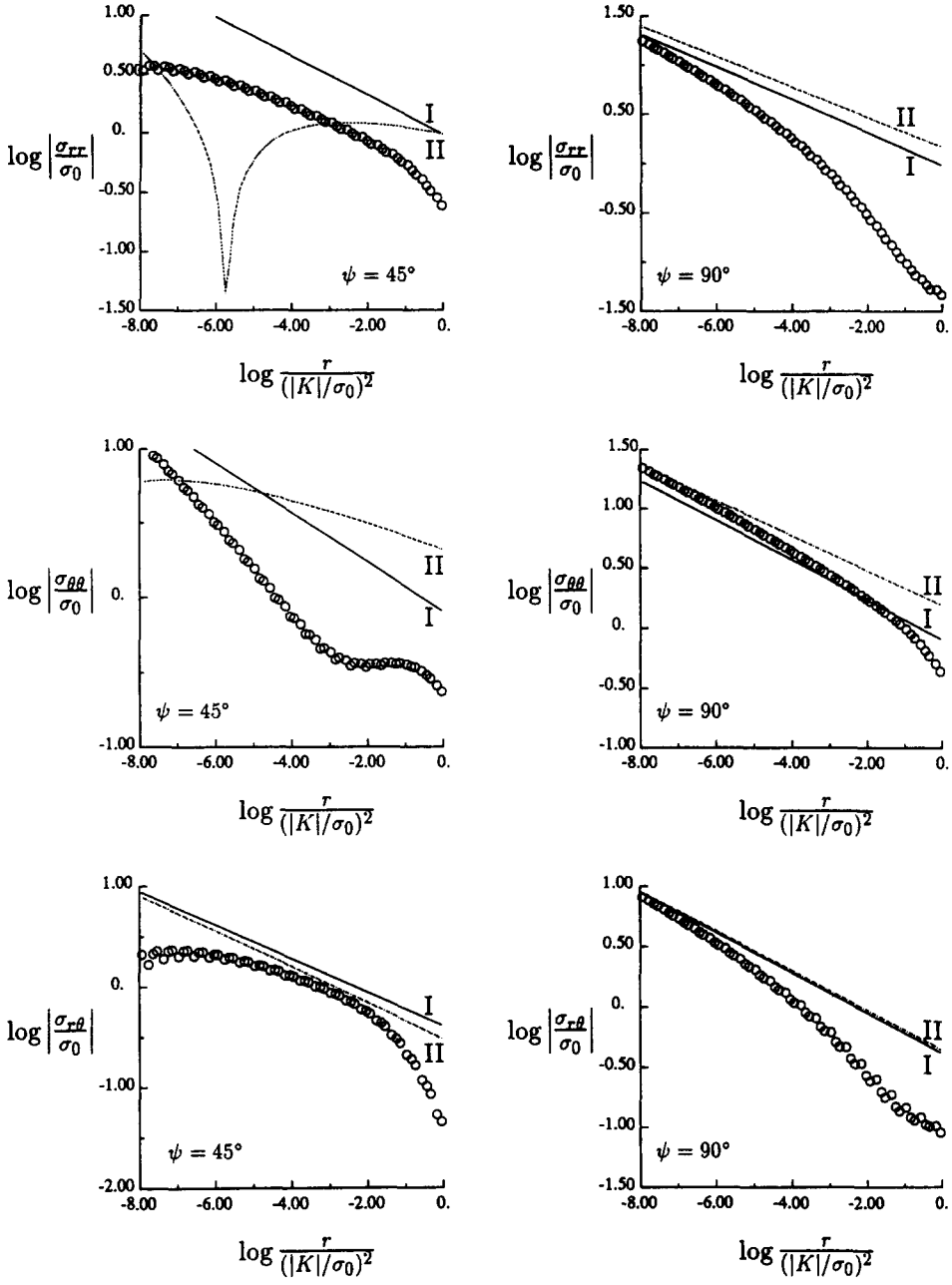

Fig. 12. *Continued.*

in Fig. 14. Perfect bonding is assumed ahead of the crack and the crack face is kept traction-free. The near-tip mesh design is similar to that described in the previous section and the radial size of the crack tip elements is $10^{-5}a$.

An incremental (flow) plasticity theory is used in this set of calculations. The elastic–plastic medium is assumed to obey the von Mises yield criterion with associated flow rule and the constitutive equation is of the form

$$\dot{\epsilon}_{ij} = \frac{1+\nu}{E}\dot{\sigma}_{ij} - \frac{\nu}{E}\delta_{ij}\dot{\sigma}_{kk} + \frac{9}{4h}\frac{s_{kl}\dot{s}_{kl}}{\sigma_y^2}s_{ij}, \tag{82}$$

where

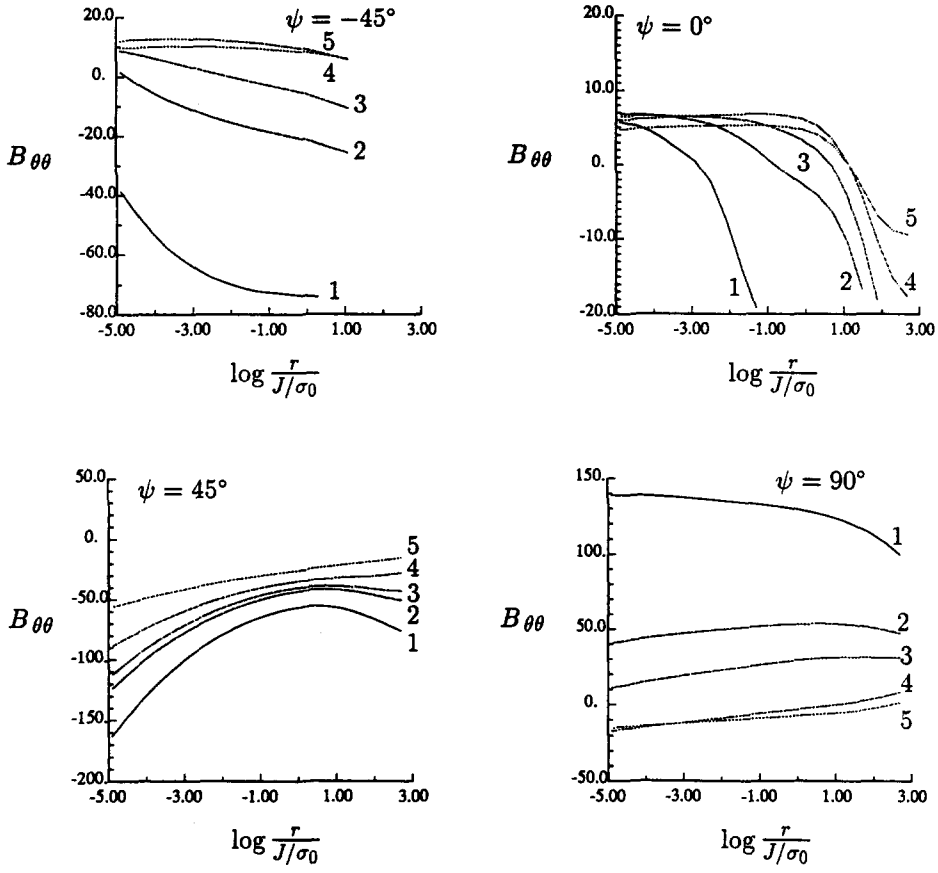

Fig. 13. Radial variation of $B_{\theta\theta}$ for the different cases analysed. Numbers 1–5 in the figure correspond to $\theta = 3.75°$, 26.25°, 41.25°, 86.25° and 131.25°.

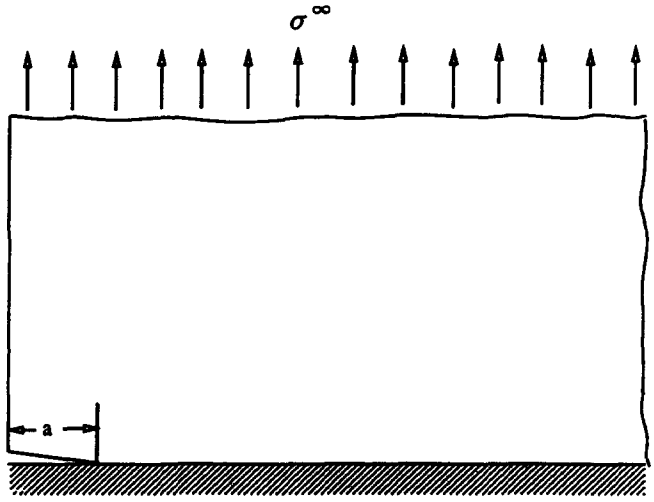

Fig. 14. Schematic representation of shallow-cracked bimaterial specimen.

$$\frac{\sigma_y}{\sigma_0} = \left(1 + \frac{\bar{\epsilon}^p}{\alpha\epsilon_0}\right)^{1/n}, \quad h = \frac{d\sigma_y}{d\bar{\epsilon}^p}, \quad \dot{\bar{\epsilon}}^p = (\tfrac{2}{3}\dot{\epsilon}^p_{ij}\dot{\epsilon}^p_{ij})^{1/2}, \tag{83}$$

σ_0 is the uniaxial yield stress of the material, $\epsilon_0 = \sigma_0/E$ is the yield strain, a superposed dot denotes material time derivative, and $\dot{\epsilon}^p$ is the plastic part of the strain rate tensor. The material constants used in the calculations are $E/\sigma_0 = 300$, $\nu = 0.3$, $n = 5$ and $\alpha = 1$.

The results presented in the following are for the final load level $\sigma^\infty = 1.2\sigma_0$.

Figure 15 shows the radial variation of the in-plane stress components along the radial lines $\theta = 3.75°$ and $41.25°$. Figure 16 depicts the angular variation of the same stress components at two different radii $r = 3.2 \times 10^{-4}a = 0.01J/\sigma_0$ and $r = 0.05a = 1.8J/\sigma_0$.

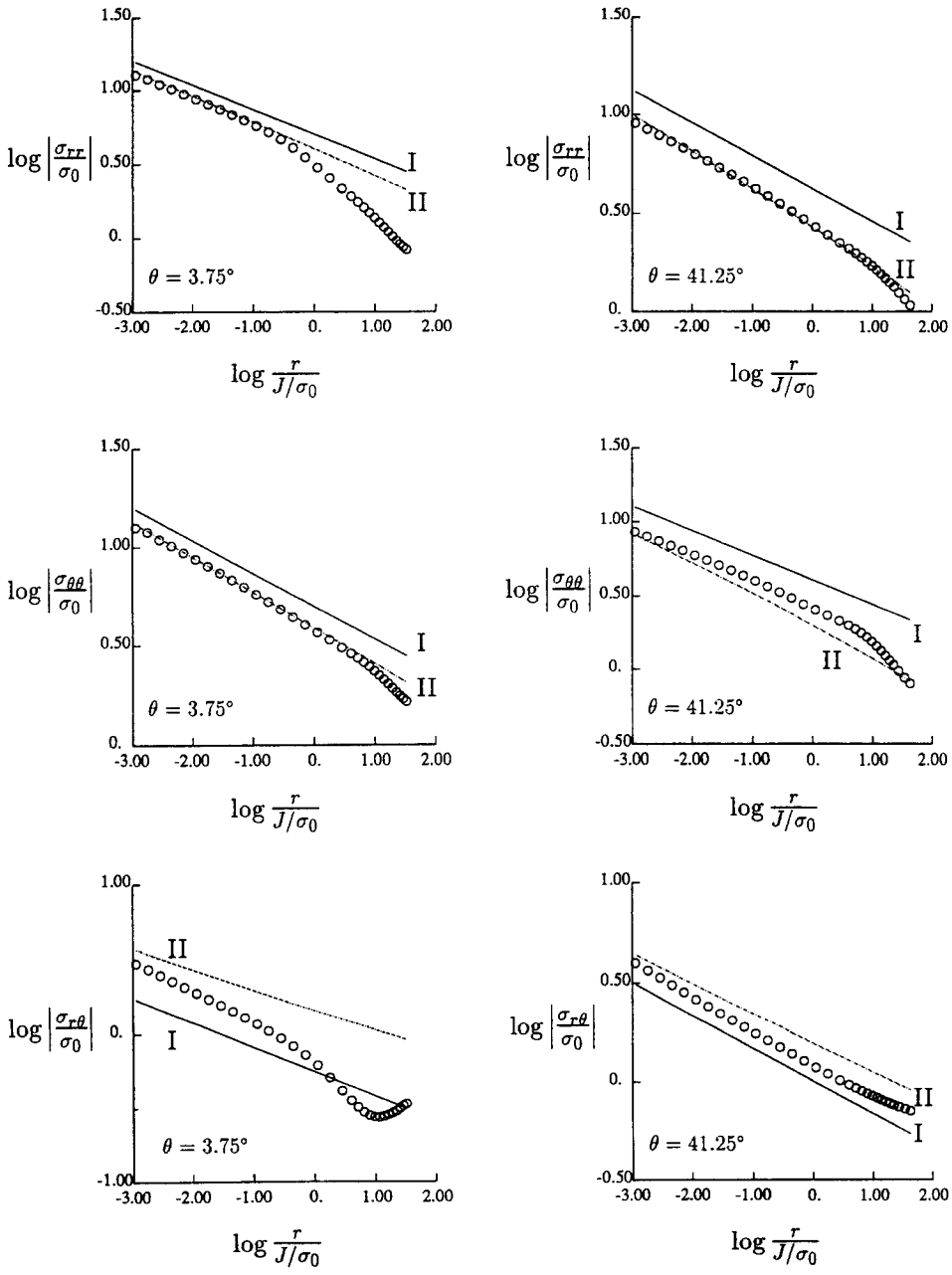

Fig. 15. Radial variation of the in-plane stress components along the radial lines $\theta = 3.75°$ and $41.25°$.

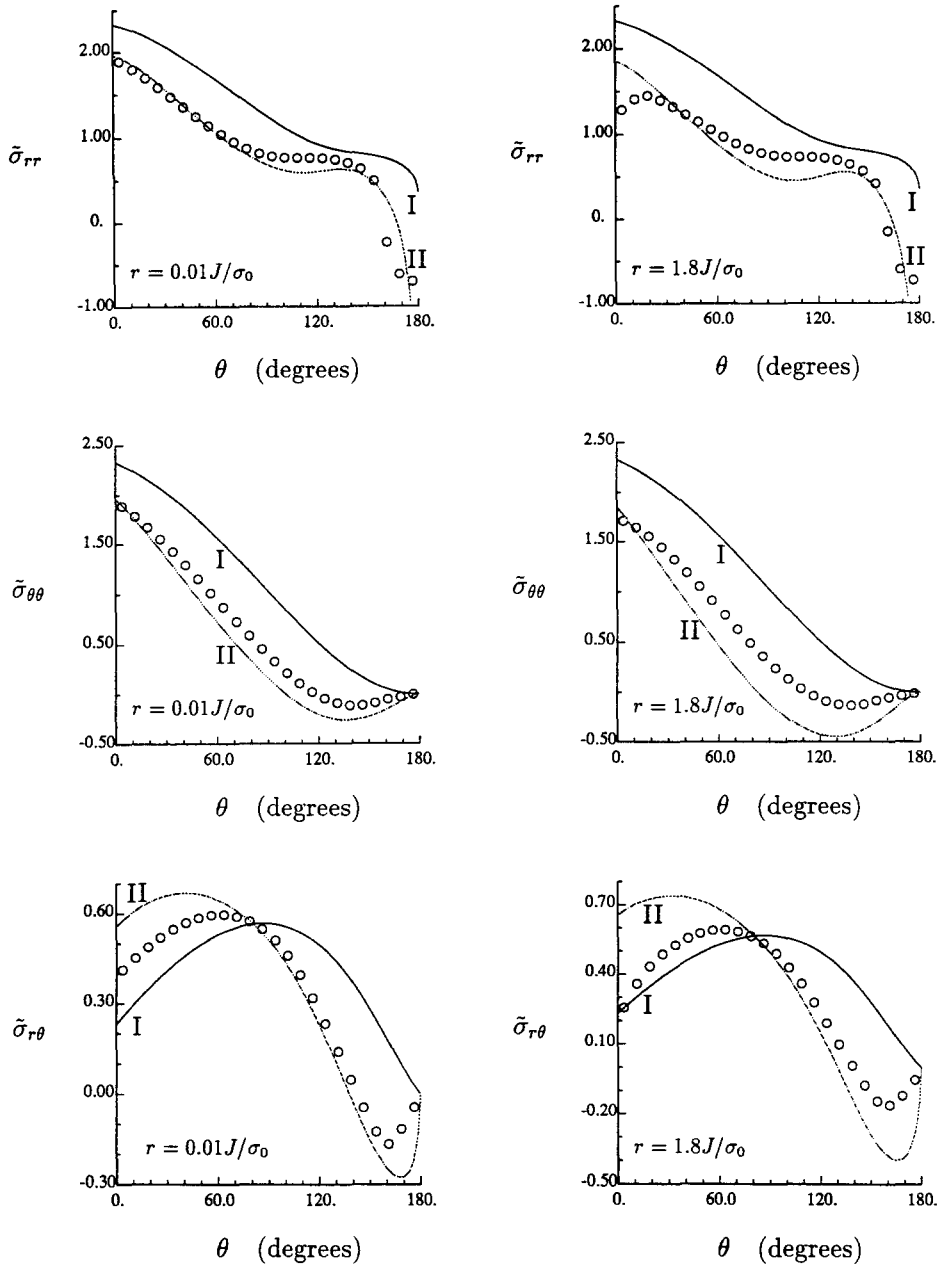

Fig. 16. Angular variation of the in-plane stress components at two different radii $r = 3.2 \times 10^{-4}a = 1.13 \times 10^{-2}J/\sigma_0$ and $r = 0.05a = 1.8J/\sigma_0$.

The value of Q used in Figs 15 and 16 is $Q = -27$ and is determined using eqn (19) together with the finite element solution.

Figures 15 and 16 show that the two-term asymptotic expansion (11) agrees well with the predictions of the finite element solution. The region of dominance of the asymptotic solution appears to be again a function of θ.

7. INTERFACIAL CREEP FRACTURE

In this section, we discuss briefly the use of the developed asymptotic solution in problems of interfacial creep fracture.

Referring to the interfacial crack tip of Fig. 1, we assume that the constitutive equation of the deformable medium is of the form

$$\dot{\epsilon}_{ij} = \frac{1+\nu}{E}\dot{s}_{ij} + \frac{1-2\nu}{3E}\dot{\sigma}_{kk}\delta_{ij} + \tfrac{3}{2}\dot{\epsilon}_0\left(\frac{\sigma_e}{\sigma_0}\right)^{n-1}\frac{s_{ij}}{\sigma_0}. \tag{84}$$

The asymptotic solution can be now written as (Riedel and Rice, 1980)

$$\frac{\boldsymbol{\sigma}(r,\theta,T)}{\sigma_0} = \left(\frac{C(T)}{\dot{\epsilon}_0\sigma_0 I_n r}\right)^{1/(n+1)}\tilde{\boldsymbol{\sigma}}^{(0)}(\theta) + Q(T)\left(\frac{r}{C(T)/\sigma_0}\right)^{t}\tilde{\boldsymbol{\sigma}}^{(1)}(\theta) + \cdots, \tag{85}$$

where T is time, $(\tilde{\boldsymbol{\sigma}}^{(0)}, \tilde{\boldsymbol{\sigma}}^{(1)}, I_n, t)$ are the same as those of eqn (11),

$$C(T) = \lim_{r\to 0}\int_0^{\pi}\left(\frac{n}{n+1}\sigma_{ij}\dot{\epsilon}_{ij}\cos\theta - n_i\sigma_{ij}\frac{\partial\dot{u}_j}{\partial x}\right)r\,\mathrm{d}\theta, \tag{86}$$

and $n_1 = \cos\theta$, $n_2 = \sin\theta$.

8. CLOSURE

In closing, we mention that the two-term asymptotic elastoplastic solution developed herein provides a suitable basis for the development of a two-parameter $(J-Q)$ fracture criterion. It should be also noted that in order to establish a sound fracture criterion, one has to make sure that the asymptotic solution, on which the fracture criterion is based, provides an accurate description of the near-tip stresses over distances larger than the fracture process zone (Hutchinson, 1983). For the case of the shallow edge crack, we find that the asymptotic solution provides an accurate description of the near tip stresses over radial distances of the order $r \simeq 2J/\sigma_0$. It is important to note, however, that the region of dominance of the asymptotic solution depends, in general, on the geometry as well as the type of loading of the structure considered. Therefore, a careful evaluation of the region of dominance of the asymptotic solution is necessary, before a specific specimen geometry is used for the determination of the interfacial fracture toughness in ductile materials.

Acknowledgements—It is a pleasure to acknowledge fruitful discussions on the discreteness of the near tip mode-mix with Professor P. Ponte Castañeda of the University of Pennsylvania. This work was carried out while both authors were supported by the NSF MRL program at the University of Pennsylvania under Grant No. DMR-9120668. The ABAQUS finite element code was made available under academic license from Hibbitt, Karlsson, and Sorensen, Inc., Providence, RI.

REFERENCES

Aravas, N. and Sharma, S. M. (1991). An elastoplastic analysis of the interface crack with contact zones. *J. Mech. Phys. Solids* **39,** 311–344.

Bose, K. and Ponte Castañeda, P. (1992). Stable crack growth under mixed mode conditions. *J. Mech. Phys. Solids* **40,** 1053–1103.

Champion, C. R. and Atkinson, C. (1990). A mode III crack at the interface between two nonlinear materials, *Proc. R. Soc. Lond.* **A429,** 247–257.

Champion, C. R. and Atkinson, C. (1991). A crack at the interface between two power-law materials under plane strain loading. *Proc. R. Soc. Lond.* **A432,** 547–553.

Comninou, M. (1977). The interface crack. *J. Appl. Mech.* **44,** 631–636.

Comninou, M. (1990). An overview of interface cracks. *Engng Fract. Mech.* **37,** 197–208.

England, A. H. (1965). A crack between dissimilar media. *J. Appl. Mech.* **32,** 400–402.

Erdogan, F. (1963). Stress distribution in a nonhomogeneous elastic plane with cracks. *J. Appl. Mech.* **30,** 232–236.

Hibbitt, H. D. (1984). ABAQUS/EPGEN—A general purpose finite element code with emphasis on nonlinear applications. *Nucl. Engng Des.* **77,** 271–297.

Hughes, T. J. R. (1980). Generalization of selective integration procedures to anisotropic and nonlinear media. *Int. J. Num. Meth. Engng* **15,** 1413–1418.

Hughes, T. J. R. (1987). *The Finite Element Method.* Prentice-Hall, Englewood Cliffs, NJ.

Hutchinson, J. W. (1968). Singular behaviour at the end of a tensile crack in a hardening material. *J. Mech. Phys. Solids* **16,** 13–31.
Hutchinson, J. W. (1983). Fundamentals of the phenomenological theory of nonlinear fracture mechanics. *J. Appl. Mech.* **50,** 1042–1051.
Hutchinson, J. W. (1990). Mixed mode fracture mechanics of interfaces. In *Metal Ceramic Interfaces* (Edited by M. Ruhle, A. G. Evans, M. F. Ashby and J. P. Hirth), pp. 295–306. Pergamon Press, Oxford.
Hutchinson, J. W. and Suo, Z. (1992). Mixed mode fracture in laminated solids. In *Advances in Applied Mechanics* (Edited by J. W. Hutchinson and T. Y. Wu), Vol. 28. Pergamon Press, Oxford (to appear).
Quanxin Guo and Keer, L. M. (1990). A crack at the interface between an elastic–perfectly plastic solid and a rigid substrate. *J. Mech. Phys. Solids* **38,** 843–857.
Rice, J. R. (1988). Elastic fracture mechanics concepts for interfacial cracks. *J. Appl. Mech.* **55,** 98–103.
Rice, J. R. and Rosengren, G. F. (1968). Plane strain deformation near a crack tip in a power-law hardening material. *J. Mech. Phys. Solids* **16,** 1–12.
Rice, J. R. and Sih, G. C. (1965). Plane problems of cracks in dissimilar media. *J. Appl. Mech.* **32,** 418–423.
Riedel, H. and Rice, J. R. (1980). Tensile cracks in creeping solids. *Fracture Mechanics: Twelfth Conference, ASTM STP 700,* 112–130.
Salganik, R. L. (1963). The brittle fracture of cemented bodies. *Priskl. Matem. Mekh.* **27,** 957–962.
Sharma, S. M. and Aravas, N. (1991a). Determination of higher order terms in asymptotic elastoplastic crack tip solutions. *J. Mech. Phys. Solids* **39,** 1043–1072.
Sharma, S. M. and Aravas, N. (1991b). Plane stress elastoplastic solutions of the interface crack with contact zones. *Mech. Mater.* **12,** 147–163.
Shih, C. F. (1974). Small-scale yielding analysis of mixed mode plane-strain crack problems. *Fracture Analysis, ASTM STP 560,* 187–210.
Shih, C. F. (1991). Cracks on bimaterial interfaces: Elasticity and plasticity aspects. *Mat. Sci. Engng* **A143,** 77–90.
Shih, C. F. and Asaro, R. J. (1988). Elastic–plastic analysis of cracks on bimaterial interfaces: Part I—Small-scale yielding. *J. Appl. Mech.* **55,** 299–316.
Shih, C. F. and Asaro, R. J. (1989). Elastic–plastic analysis of cracks on bimaterial interfaces: Part II—Structure of small-scale yielding fields. *J. Appl. Mech.* **56,** 763–779.
Shih, C. F. and Asaro, R. J. (1991). Elastic–plastic analysis of cracks on bimaterial interfaces: Part III—Large-scale yielding fields. *J. Appl. Mech.* **58,** 450–463.
Wang, T. C. (1990). Elastic–plastic asymptotic fields for cracks on bimaterial interfaces. *Engng Fract. Mech.* **37,** 527–538.
Williams, M. L. (1959). The stresses around a fault or crack in dissimilar media. *Bull. Seis. Soc. Am.* **49,** 199–204.
Wolfram, S. (1991). *Mathematica* (2nd Edn). Addison-Wesley, Reading, MA.
Yuli Gao and Zhiwen Lou (1990). Mixed mode interface crack in a pure power-hardening bimaterial. *Int. J. Fract.* **43,** 241–256.
Zywicz, E. and Parks, D. M. (1990). Elastic–plastic analysis of frictionless contact at interfacial crack tips. *Int. J. Fract.* **42,** 129–143.
Zywicz, E. and Parks, D. M. (1992). Small-scale yielding interfacial crack tip fields. *J. Mech. Phys. Solids* **40,** 511–536.

APPENDIX A

The matrix $\mathbf{F}(s)$ used in eqn (35) is given by

$$\mathbf{F}(s) = \begin{pmatrix} 0 & -s & 0 & 3 \\ -(s+2) & 0 & 0 & 0 \\ 0 & 0 & 0 & -(s+2) \\ -(4/3)(s+1)^2 & 0 & -s & 0 \end{pmatrix}.$$

The matrix $\mathbf{G}(\mathbf{x}, s)$ on the right-hand side of (35) is written as $\mathbf{G}(\mathbf{x}, s) = \mathbf{G}^{(0)}(\mathbf{x}, s) + O(\epsilon)$, where

$$\mathbf{G}^{(0)}(\mathbf{x}, s) = \begin{pmatrix} 0 & -s & 0 & 3\ln\tilde{\sigma}_e^{(0)} \\ -s & 0 & 0 & 0 \\ 0 & 0 & 0 & 0 \\ (4/3)(s+1)[(s+1)\ln\tilde{\sigma}_e^{(0)} - s] & 0 & 0 & 0 \end{pmatrix}.$$

The columns of matrix $\boldsymbol{\Psi}$ are the fundamental solutions of the homogeneous version of equation (35), i.e.

$$\boldsymbol{\Psi}(\theta, s) = \begin{pmatrix} a\sin(s\theta) & -a\cos(s\theta) & \cos[(2+s)\theta] & \sin[(2+s)\theta] \\ b\cos(s\theta) & b\sin(s\theta) & -\sin[(2+s)\theta] & \cos[(2+s)\theta] \\ -c\sin(s\theta) & c\cos(s\theta) & -d\cos[(2+s)\theta] & -d\sin[(2+s)\theta] \\ \cos(s\theta) & \sin(s\theta) & -d\sin[(2+s)\theta] & d\cos[(2+s)\theta] \end{pmatrix},$$

where $a = 1.5/(1+s)$, $b = ac$, $c = (2+s)/s$ and $d = 1/a$.

The solution $\mathbf{x}^{(0)}$ is given by

$$x_1^{(0)} = \frac{A_I}{4}\left(-3\sin\frac{\theta}{2}+9\sin\frac{3\theta}{2}\right)+\frac{A_{II}}{4}\left(3\cos\frac{\theta}{2}-3\cos\frac{3\theta}{2}\right),$$

$$x_2^{(0)} = \frac{A_I}{4}\left(-9\cos\frac{\theta}{2}+9\cos\frac{3\theta}{2}\right)+\frac{A_{II}}{4}\left(-9\sin\frac{\theta}{2}+3\sin\frac{3\theta}{2}\right),$$

$$x_3^{(0)} = \frac{A_I}{4}\left(-3\sin\frac{\theta}{2}-3\sin\frac{3\theta}{2}\right)+\frac{A_{II}}{4}\left(3\cos\frac{\theta}{2}+\cos\frac{3\theta}{2}\right),$$

$$x_4^{(0)} = \frac{A_I}{4}\left(\cos\frac{\theta}{2}+3\cos\frac{3\theta}{2}\right)+\frac{A_{II}}{4}\left(\sin\frac{\theta}{2}+\sin\frac{3\theta}{2}\right).$$

Next, we write

$$\tilde{\boldsymbol{\sigma}}^{(0)}(\theta) = \boldsymbol{\Sigma}^{(0)}(\theta)+O(\epsilon),$$

where $\boldsymbol{\Sigma}^{(0)}$ is found using $x_3^{(0)}$ and $x_4^{(0)}$, and define

$$\Sigma_e^{(0)} = (\tfrac{3}{2}S_{ij}^{(0)}S_{ij}^{(0)})^{1/2},$$

where $\mathbf{S}^{(0)}$ is the deviatoric part of $\boldsymbol{\Sigma}^{(0)}$.

Finally, the functions I_1 and I_2 in (45) and (46) are defined as

$$I_1 = \int_0^{\pi}\sin\theta\left[\frac{A_{II}}{A_I}(1+3\cos 2\theta)+\sin 2\theta\right]\ln[\Sigma_e^{(0)}(\theta)]\,d\theta,$$

and

$$I_2 = \int_0^{\pi}\left[\frac{A_{II}}{A_I}(7\cos\theta+9\cos 3\theta)+(-\sin\theta+3\sin 3\theta)\right]\ln[\Sigma_e^{(0)}(\theta)]\,d\theta.$$

APPENDIX B

In order to simplify the expressions given below, we write

$$\tilde{\boldsymbol{\sigma}}^{(0)}(\theta) = \boldsymbol{\Sigma}^{(0)}(\theta)+\epsilon\boldsymbol{\Sigma}^{(1)}(\theta)+O(\epsilon^2),$$

where $\boldsymbol{\Sigma}^{(0)}$ and $\boldsymbol{\Sigma}^{(1)}$ are known from the solution $\mathbf{x}^{(0)}$ and $\mathbf{x}^{(1)}$. Also, we define

$$\Sigma_e^{(0)} = (\tfrac{3}{2}S_{ij}^{(0)}S_{ij}^{(0)})^{1/2} \quad \text{and} \quad \Sigma_e^{(1)} = \frac{3}{2}\frac{S_{ij}^{(0)}S_{ij}^{(1)}}{\Sigma_e^{(0)}},$$

where $(\mathbf{S}^{(0)}, \mathbf{S}^{(1)})$ are the deviatoric parts of $(\boldsymbol{\Sigma}^{(0)}, \boldsymbol{\Sigma}^{(1)})$.

The matrix $\hat{\mathbf{G}}(\theta, t)$ on the right-hand side of (47) is written as $\hat{\mathbf{G}}(\theta,t) = \hat{\mathbf{G}}^{(0)}(\theta,t)+\epsilon\hat{\mathbf{G}}^{(1)}(\theta,t)+O(\epsilon^2)$, with

$$\hat{\mathbf{G}}^{(0)}(\theta,t) = \begin{pmatrix} 6(t+1)X(\theta) & 1/2 & 0 & 3R(\theta) \\ 1/2 & 0 & 0 & 0 \\ 0 & 0 & 0 & 0 \\ (2/3)(t+1)[2(t+1)Z(\theta)+1] & 0 & 0 & 6(t+1)X(\theta) \end{pmatrix}$$

and

$$\hat{\mathbf{G}}^{(1)}(\theta,t) = \begin{pmatrix} 3X(\theta)[2(t+1)Y(\theta)-1] & -1/4 & 0 & 3T(\theta) \\ -1/4 & 0 & 0 & 0 \\ 0 & 0 & 0 & 0 \\ -(1/3)(t+1)[1+2Z(\theta)-4(t+1)P(\theta)] & 0 & 0 & 6(t+1)X(\theta)Y(\theta) \end{pmatrix},$$

where

$$X = \frac{S_{rr}^{(0)}\Sigma_{r\theta}^{(0)}}{\Sigma_e^{(0)2}},$$

$$Y = \frac{\Sigma_{r\theta}^{(1)}}{\Sigma_{r\theta}^{(0)}}+\frac{S_{rr}^{(1)}}{S_{rr}^{(0)}}-2\frac{\Sigma_e^{(1)}}{\Sigma_e^{(0)}}-3\frac{S_{rr}^{(0)2}}{\Sigma_e^{(0)2}},$$

$$Z = m+3\frac{S_{rr}^{(0)2}}{\Sigma_e^{(0)2}},$$

$$P = \frac{\Sigma_e^{(1)}}{\Sigma_e^{(0)}} + \frac{m^2}{2} + 6\frac{S_{rr}^{(0)2}}{\Sigma_e^{(0)2}}\left(\frac{S_{rr}^{(1)}}{S_{rr}^{(0)}} - \frac{\Sigma_e^{(1)}}{\Sigma_e^{(0)}} + \frac{m}{2}\right) - Z^2,$$

$$R = m + 3\frac{\Sigma_{r\theta}^{(0)2}}{\Sigma_e^{(0)2}},$$

$$T = \frac{m^2}{2} + \frac{\Sigma_e^{(1)}}{\Sigma_e^{(0)}} + 6\frac{\Sigma_{r\theta}^{(0)2}}{\Sigma_e^{(0)2}}\left(\frac{\Sigma_{r\theta}^{(1)}}{\Sigma_{r\theta}^{(0)}} - \frac{\Sigma_e^{(1)}}{\Sigma_e^{(0)}}\right) + 3m\frac{\Sigma_{r\theta}^{(0)2}}{\Sigma_e^{(0)2}} - 9X^2,$$

$$m = \ln \Sigma_e^{(0)}.$$

The solution $\mathbf{y}^{(0)}$ is identical to $\mathbf{x}^{(0)}$ with (A_I, A_{II}) replaced by (B_I, B_{II}). Finally, the solution $\mathbf{y}^{(1)}$ is given by

$$y_1^{(1)} = \tfrac{1}{4}B_I \sin\frac{\theta}{2}\left[1 - \cos\theta + (1 + 3\cos\theta)\ln\left(3\sin^2\frac{\theta}{2}\right)\right] + \tfrac{1}{4}B_{II}\sin\frac{\theta}{2}\sin\theta\ln\left(3\sin^2\frac{\theta}{2}\right),$$

$$y_2^{(1)} = \tfrac{1}{2}B_I \cos\frac{\theta}{2}\sin^2\frac{\theta}{2}\left[4 - 3\ln\left(3\sin^2\frac{\theta}{2}\right)\right] + \tfrac{1}{2}B_{II}\sin^3\frac{\theta}{2}\left[1 - \ln\left(3\sin^2\frac{\theta}{2}\right)\right],$$

$$y_3^{(1)} = \tfrac{1}{2}B_I \sin\frac{\theta}{2}\cos^2\frac{\theta}{2}\left[-1 + 6\ln\left(\cos\frac{\theta}{2}\right)\right] - B_{II}\cos^3\frac{\theta}{2}\ln\left(\cos\frac{\theta}{2}\right),$$

$$y_4^{(1)} = \tfrac{1}{2}B_I \cos\frac{\theta}{2}\left[1 - \cos\theta + (1 - 3\cos\theta)\ln\left(\cos\frac{\theta}{2}\right)\right] - \tfrac{1}{4}B_{II}\sin\theta\cos\frac{\theta}{2}\left[1 + 2\ln\left(\cos\frac{\theta}{2}\right)\right].$$